ARMY RESEARCH LABORATORY

Dynamic Experiments and Constitutive Model Performance for Polycarbonate

by Stephan R. Bilyk

ARL-TR-6937 **July 2014**

NOTICES

Disclaimers

The findings in this report are not to be construed as an official Department of the Army position unless so designated by other authorized documents.

Citation of manufacturer's or trade names does not constitute an official endorsement or approval of the use thereof.

Destroy this report when it is no longer needed. Do not return it to the originator.

Army Research Laboratory
Aberdeen Proving Ground, MD 21005-5069

ARL-TR-6937 **July 2014**

Dynamic Experiments and Constitutive Model Performance for Polycarbonate

Stephan R. Bilyk
Weapons and Materials Research Directorate, ARL

REPORT DOCUMENTATION PAGE

Form Approved
OMB No. 0704-0188

1. REPORT DATE *(DD-MM-YYYY)*	2. REPORT TYPE	3. DATES COVERED (From - To)
July 2014	Final	January 2013–September 2013

4. TITLE AND SUBTITLE
Dynamic Experiments and Constitutive Model Performance for Polycarbonate

5a. CONTRACT NUMBER

5b. GRANT NUMBER

5c. PROGRAM ELEMENT NUMBER

6. AUTHOR(S)
Stephan R. Bilyk

5d. PROJECT NUMBER
FPEC

5e. TASK NUMBER

5f. WORK UNIT NUMBER

7. PERFORMING ORGANIZATION NAME(S) AND ADDRESS(ES)
U.S. Army Research Laboratory
ATTN: RDRL-WMP-C
Aberdeen Proving Ground, MD 21005-5069

8. PERFORMING ORGANIZATION REPORT NUMBER
ARL-TR-6937

9. SPONSORING/MONITORING AGENCY NAME(S) AND ADDRESS(ES)

10. SPONSOR/MONITOR'S ACRONYM(S)

11. SPONSOR/MONITOR'S REPORT NUMBER(S)

12. DISTRIBUTION/AVAILABILITY STATEMENT
Approved for public release; distribution is unlimited.

13. SUPPLEMENTARY NOTES

14. ABSTRACT

An experimental and numerical investigation has been performed to examine material deformation of polycarbonate (PC) from low (quasi-static) to high (dynamic) strain rates. In 2012, a revised physics-based constitutive model for thermoplastics was implemented into several U.S. Department of Energy (DOE) hydrocodes at the U.S. Army Research Laboratory. This report briefly describes the Mulliken-Boyce (M-B) amorphous polymer model and reviews significant modifications in implementation for DOE hydrocodes. The original material model parameters obtained for the M-B model only considered isothermal deformations of PC, while a subsequent implementation of M-B into the finite element code LS-DYNA obtained material parameters for adiabatic heating. Observed results are used in this report for validation and to examine performance differences in the mentioned model parameter sets. Dynamic-Tensile-Extrusion is an integrated experimental technique that allows the study of material deformation at high strain rates (greater than10,000/s) and large strains (greater than 1) when subjected to dynamic tension loading conditions. This is an important complement to the more traditional Taylor cylinder impact experiment, which achieves large strain and high-strain-rate deformation but under hydrostatic compression. Additionally, model parameter sensitivity is evaluated herein by considering pressure dependence of flow strength and its influence for amorphous polymer materials subjected to hydrostatic tension or compression.

15. SUBJECT TERMS
amorphous polymers, Mulliken-Boyce model, rate dependent, pressure dependent, parameter sensitivity

16. SECURITY CLASSIFICATION OF:			17. LIMITATION OF ABSTRACT	18. NUMBER OF PAGES	19a. NAME OF RESPONSIBLE PERSON
a. REPORT	b. ABSTRACT	c. THIS PAGE			Stephan R. Bilyk
Unclassified	Unclassified	Unclassified	UU	44	19b. TELEPHONE NUMBER (*Include area code*) 410-278-2976

Standard Form 298 (Rev. 8/98)
Prescribed by ANSI Std. Z39.18

Contents

List of Figures **iv**

List of Tables **vi**

Acknowledgments **vii**

1. Introduction **1**

2. Materials and Experimental Methods **3**

3. Constitutive Model **7**

4. Numerical Considerations **12**

5. Results **14**

5.1 Dynamic Compression 16

5.2 Dynamic Tension 23

6. Summary, Conclusions and Recommendations **30**

7. References **32**

Distribution List **34**

List of Figures

Figure 1. In situ x-ray absorption characterization of shaped charge jet/target interaction. Performed at ARL EF-7; courtesy of M. Zellner, ARL. 2

Figure 2. Dramatic change in mechanical properties for amorphous polymers as the temperature passes through glass transition, T_g. 3

Figure 3. Original schematic of a Taylor impact experiment. 4

Figure 4. (a) Schematic of the Dyn-Ten-Ext experiment and (b) sequenced high-speed video frames of the sample event. 4

Figure 5. Schematic of the single stage gas gun used for the Taylor cylinder impact experiments at MIT ISN. The assembly shown is for an impact-penetration experiment using a finite thickness target. 5

Figure 6. Hemishere-ended cylinder samples and directionality considered for polycarbonate as used for DynTen-Ext experiments. 7

Figure 7. Storage and loss tangent moduli for PC; DMA experiments performed at 1 Hz and shift at 100 Hz showing the α and β transition regions using the Deconstruct-Shift-Reconstruct analytical method. 8

Figure 8. (a) Observed uniaxial compression response of PC over a range of strain rates performed at room temperature; (b) strain rate sensitivity of flow stress. 9

Figure 9. One-dimensional (1-D) depiction of the M-B constitutive model. The spring in segment B is a strain hardening Langevin (nonlinear) spring representing chain stretching and alignment; the springs in segment A are rate- and temperature-dependent elastic (linear) springs and the dashpots represent rate-, temperature-, and pressure-dependent viscoplastic terms for intermolecular resistance. 10

Figure 10. Comparison of PC material response in uniaxial compression using the M-B model for parameters obtained assuming isothermal conditions (labeled Mulliken and Boyce in plot) and modified parameters for plastic work (labeled Varghese and Batra in plot). 12

Figure 11. Schematic illustrating the reference configuration, initial conditions, and boundary conditions used for the ALE3D Taylor cylinder impact simulations. 13

Figure 12. Schematic illustrating the reference configuration, initial conditions, and boundary conditions used for the ALE3D Dyn-Ten-Ext simulations 13

Figure 13. High-speed video frames recorded at various stages during a Taylor cylinder impact experiment on a 76.2-mm PC rod at 187 m/s. Note elastic recovery after 100 μs and rebound (detachment from rigid surface) at 198 μs. 17

Figure 14. Parameter sensitivity showing numerical contours of axial stress using the M-B model for a Taylor cylinder impact experiment at a striking velocity of 187 m/s (labeled D2) at sequential times after rigid impact. (a) Full original parameters used in M-B, (b) full VBB parameters used in M-B, (c) VBB parameters used in M-B with the viscoplastic α phase disabled, (d) VBB parameters used in M-B with the viscoplastic β phase disabled, (e) VBB parameters used in M-B with pressure dependence of strength disabled, (f) comparison of temperature rise due to plastic work-to-heat conversion near end of impact event using (i) full VBB parameters in M-B, (ii) α phase disabled, (iii) β phase disabled, (iv) pressure dependence disabled.....18

Figure 15. Parameter sensitivity showing numerical contours of strain rate using the M-B model for a Taylor cylinder impact experiment at a striking velocity of 187 m/s (labeled S2) at sequential times after rigid impact. (a) Full original parameters used in M-B, (b) full VBB parameters used in M-B, (c) VBB parameters used in M-B with the viscoplastic α phase disabled, (d) VBB parameters used in M-B with the viscoplastic β phase disabled, and (e) VBB parameters used in M-B with pressure dependence of strength disabled. 20

Figure 16. Parameter sensitivity showing pressure contours using the M-B model for a Taylor cylinder impact experiment at a striking velocity of 187 m/s (labeled S2) at sequential times after rigid impact. (a) Full original parameters used in M-B, (b) full VBB parameters used in M-B, (c) VBB parameters used in M-B with the viscoplastic α phase disabled, (d) VBB parameters used in M-B with the viscoplastic β phase disabled, and (e) VBB parameters used in M-B with pressure dependence of strength disabled. 21

Figure 17. Comparison of strain hardening due to chain stretching for PC striking a rigid anvil at 187 m/s. Deformed shape and contours shown at the end of impact event for (a) experiment, (b) full VBB parameters, (c) VBB parameters with pressure dependence of strength disabled, (d) VBB parameters used in M-B with the viscoplastic α phase disabled, and (e) VBB parameters used in M-B with the viscoplastic β phase disabled.....22

Figure 18. Recovered .30-caliber specimens from Dyn-Ten-Ext experiments for PC. (a) Arrested intact specimen from low velocity impact (less than 350 m/s), showing necking, void nucleation behind the neck, and circumferential fracture behind the void. (b) Comparison of arrested intact specimen and failed specimen (upper is low velocity, lower is high velocity), where central voiding and peripheral fracture have proceeded nearly to complete failure. There is a small ligament of unfractured material remaining in the failed part. 24

Figure 19. Dyn-Ten-Ext experiment for PC as captured at the die exit by a Shimadzu high-speed framing camera. The time in microseconds from camera trigger is noted in the lower-right corner of the images (18, 40, 98, and 198 μs, respectively). The test conditions were striking velocity of 523 m/s with a die exit of 0.36 cm. PC failure is in the corkscrew fracture/tearing mode. While it appears to behave in a molten fashion, the recovered pieces were found to have retracted almost to their original shape, indicating solid behavior.....25

Figure 20. Recovered .30-caliber specimens from Dyn-Ten-Ext experiments for PC showing nearly complete elastic recovery (rebound) at 363 m/s; deformation near the exiting tip at 451 m/s; and failure with fracture above 600 m/s.....25

Figure 21. Parameter sensitivity showing numerical contours of velocity using the M-B model for a Dyn-Ten-Ext experiment at a striking velocity of 363 m/s at sequential times

after die impact. (a) Full VBB parameters used in M-B, (b) VBB parameters used in M-B with pressure dependence of strength disabled, (c) VBB parameters used in M-B with the viscoplastic α phase disabled, and (d) VBB parameters used in M-B with the viscoplastic β phase disabled. 27

Figure 22. Parameter sensitivity showing numerical contours of radial stress using the M-B model for a Dyn-Ten-Ext experiment at a striking velocity of 363 m/s at sequential times after die impact. (a) Full VBB parameters used in M-B, (b) VBB parameters used in M-B with pressure dependence of strength disabled, (c) VBB parameters used in M-B with the viscoplastic α phase disabled, and (d) VBB parameters used in M-B with the viscoplastic β phase disabled. Note, positive stress is tensile and negative is compressive....28

Figure 23. Parameter sensitivity showing numerical contours of axial stress using the M-B model for a Dyn-Ten-Ext experiment at a striking velocity of 363 m/s at sequential times after die impact. (a) Full VBB parameters used in M-B, (b) VBB parameters used in M-B with pressure dependence of strength disabled, (c) VBB parameters used in M-B with the viscoplastic α phase disabled, and (d) VBB parameters used in M-B with the viscoplastic β phase disabled. Note, positive stress is tensile and negative is compressive....29

List of Tables

Table 1. M-B model parameters for PC. 16

Acknowledgments

The author is indebted to invaluable technical conversations and advice provided by Dr. Richard C. Becker. The author would also like to thank Dr. Adam D. Mulliken for courteously providing the experimental results and the Abaqus version of the model and Professor Romesh C. Batra, Virginia Polytechnic Institute and State University, for the revised model and parameters. The experiments would not have been possible without the expertise provided by Dr. Jevan Furmanski, Exxon, United States Military Academy Cadet James Tyler, Dr. G. "Rusty" Gray, Dr. Carl Trujillo, and Daniel T. Martinez, LANL MST-8. It is my honor to work and collaborate with such talented and highly intelligent individuals.

INTENTIONALLY LEFT BLANK.

1. Introduction

Materials often exhibit phenomena on a broad range of spatial and temporal scales that combine together to dictate deformation response to subsequent failure. The physical processes and evolution are complicated and may be difficult to access experimentally. Because of the complex processes present during a ballistic impact event, it is often difficult to identify the armor or material parameters that significantly influence performance. These controlling parameters can be identified using a canonical approach by performing carefully instrumented impact experiments, examination of dominant parameters in analytical and numerical penetration mechanics solutions, and/or computational modeling of the ballistic impact event (*1, 2*). Once limiting performance parameters and defeat mechanisms are identified, the armor designer can seek to control these aspects for optimized and enhanced armor performance.

Survivability of the U.S. Army's fighting forces relies on lightweight armor systems capable of sustaining multi-hit impacts. Emerging armor systems utilize multiple material components (e.g., metals, ceramics, polymers) that achieve mass and space efficiencies with improved energy absorption and durability. Further dramatic armor improvements including fast response to adaptive threats require implementing relevant material response and deformation mechanisms into hydrocodes, providing researchers the ability to identify key interactions (e.g., properties, wave propagation, interfaces, geometry, composition, processing) that pilot valued protection performance functions (e.g., stop threat, modular, rapid install and remove). For polymer selection and formulation, information relating key material properties to performance is limited. In this work, in situ dynamic behavior for polycarbonate (PC) is investigated using experimental and numerical capabilities developed at the U.S. Army Research Laboratory (ARL), Los Alamos National Laboratory (LANL), Massachusetts Institute of Technology (MIT) and Virginia Polytechnic Institute and State University (VA Tech). Properties evaluated and tested include pressure sensitivity, strain rate sensitivity, and temperature dependence. The observed results and parameter sensitivity are presented to validate a new physics-based polymer material model implemented into the U.S. Department of Energy (DOE) hydrocode ALE3D (*3*), developed at Lawrence Livermore National Laboratory (LLNL).

Amorphous glassy polymers are versatile materials that can be easily worked, molded, and thermoformed. They are effective materials for use in numerous applications requiring mechanical performance subjected to high-strain-rate loading conditions, ranging from golf balls to laminated blast/bullet-proof transparent windshields. Thermoplastic polymers have also been evaluated against high velocity chemical energy shaped charge jets, as shown in figure 1. Information relating polymer properties to performance at these extreme environments is limited. Our canonical strategy at ARL for polymers is to identify key mechanisms for protection

performance, develop and validate physics-based constitutive models, and then transfer the numerical capabilities to protection design engineers.

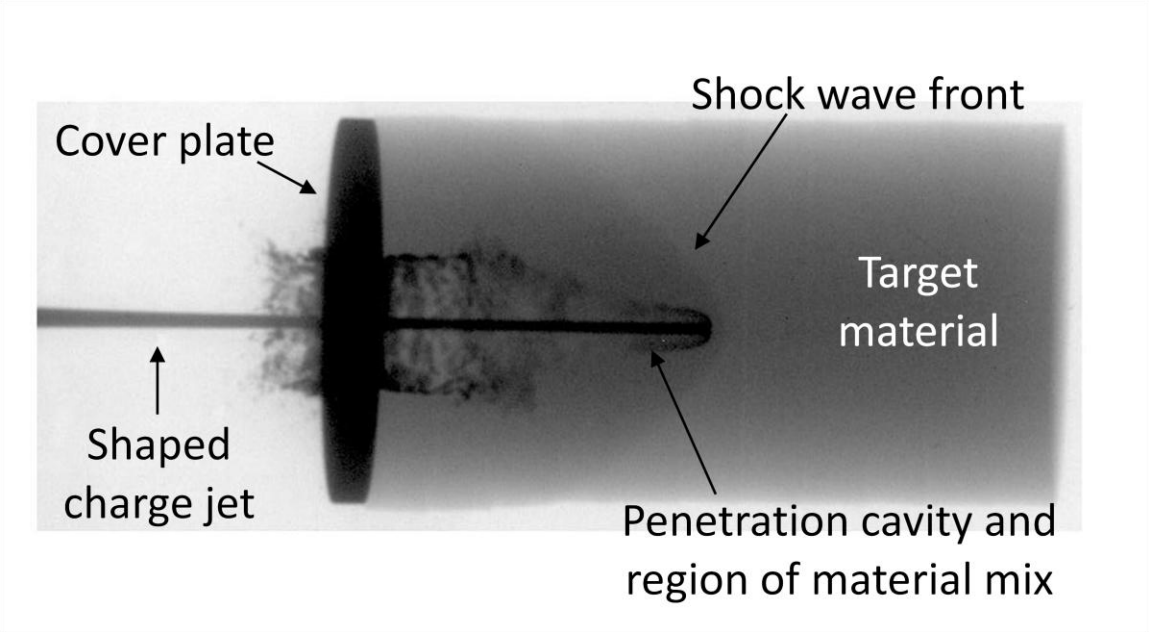

Figure 1. In situ x-ray absorption characterization of shaped charge jet/target interaction. Performed at ARL EF-7; courtesy of M. Zellner, ARL.

Mechanical properties for amorphous glassy polymers are highly influenced by the glass transition temperature, as shown in figure 2. Glassy polymers are generally soft and ductile above T_g (rubber-like state), and hard and brittle below T_g (glass-like state). The ductility under pressure is the primary reason for high impact resistance, which allows structures made of these materials to undergo large deformation before failure (*4*). Additionally, the nonlinear viscoelastic and viscoplastic behavior of amorphous polymers permit the material to transform impact energy into heat or internal energy. Glassy polymers exhibit pressure dependence of modulus and flow strength where strength increases with increasing strain rate and pressure. Because of these properties, PCs find many applications. Therefore, selection and formulation of PC for performance in specific protection technologies can be guided by identifying key material properties (pressure sensitivity, rate sensitivity, and temperature dependence).

This research effort will briefly review the thermo-elasto-viscoplastic Mulliken-Boyce (M-B) constitutive model for amorphous glassy polymers, significant modifications for model implementation into ALE3D, and an evaluation of PC material model parameters including parameter sensitivity of pressure and strain rate dependence on flow strength as compared with observed results. It provides insight into the inner-workings of the M-B model that will guide engineers and scientists for application of the constitutive model toward innovative lightweight hybrid protection design technologies for the U.S. Army.

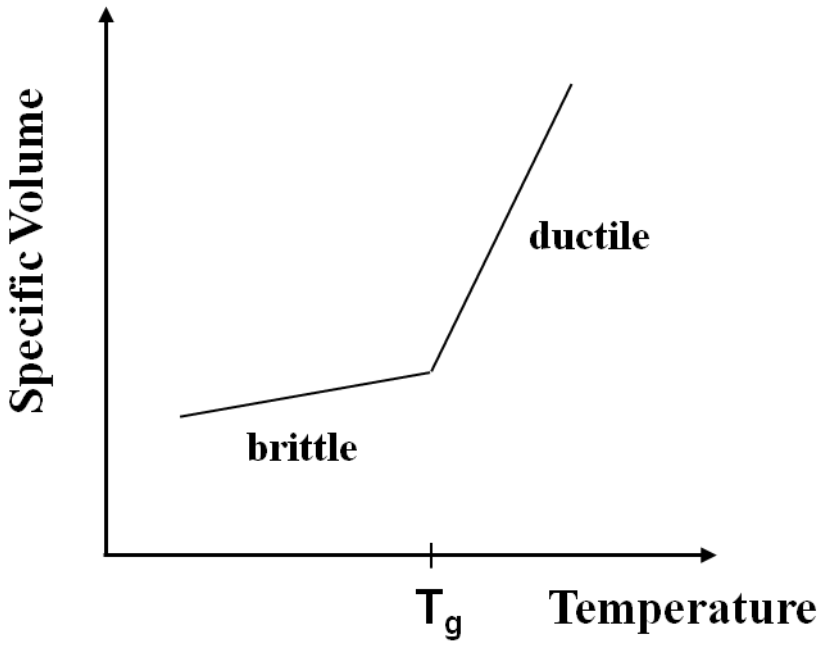

Figure 2. Dramatic change in mechanical properties for amorphous polymers as the temperature passes through glass transition, T_g.

2. Materials and Experimental Methods

Few experimental approaches are available for unambiguously assessing the deformation response of materials under extreme mechanical loading conditions, i.e., simultaneous large strains, ε greater than 1, and high strain rates, dε/dt greater than 10,000/ s (*5*). Ultra-high strain rates can be achieved during plate impact experiments, but these require elaborate experimental and specimen preparation techniques.

For the Taylor cylinder impact experimental method, a right circular cylinder is fired at high velocity onto a hard (rigid) surface, as shown in figure 3. This classic ballistic experiment was named after Sir G. I. Taylor, who developed the experiment in 1948 to screen materials for ballistic applications during World War II. Taylor recognized that this experimental procedure permitted an estimate of a dynamic yield stress by measuring the overall length of the reference or original state of the cylinder and the final deformed specimen length (*6*). Currently, the Taylor cylinder impact experiment is primarily used as a valuable tool to validate constitutive models for various ductile materials subjected to dynamic compressive loading conditions. Although the experiment is relatively simple in theory, great attention must be given to maintaining planar impact of the cylinder on the rigid anvil and accurate post-mortem analysis (*7*).

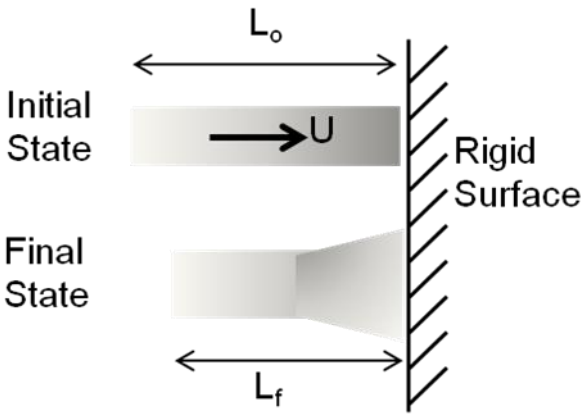

Figure 3. Original schematic of a Taylor impact experiment (*1*).

The Dynamic-Tensile-Extrusion (Dyn-Ten-Ext) experiment was developed by G. T. Gray III and coworkers at LANL to examine extreme tensile conditions in materials (*8*, *9*). The apparatus utilizes the same hardware as a Taylor cylinder impact experiment, except that a conical extrusion die is fixed to the end of the gun barrel, forcing the specimen to extrude through it at a high velocity (see figure 4 [a]), and the anvil is not employed. The leading edge velocity of the specimen is relatively unaffected by the extrusion process, but the trailing portion rapidly decelerates inside the die, and thus the extruded ligament at the die exit is pulled in high strain rate tension, typically to large strains and, ultimately, to failure (see figure 4 [b]). As an integrated experiment that generates extreme dynamic tensile deformation, Dyn-Ten-Ext provides a complementary means to challenge the quantitative accuracy of constitutive models parameterized under less extreme conditions. It also reveals tensile and shear instabilities that are not active in dynamic compression.

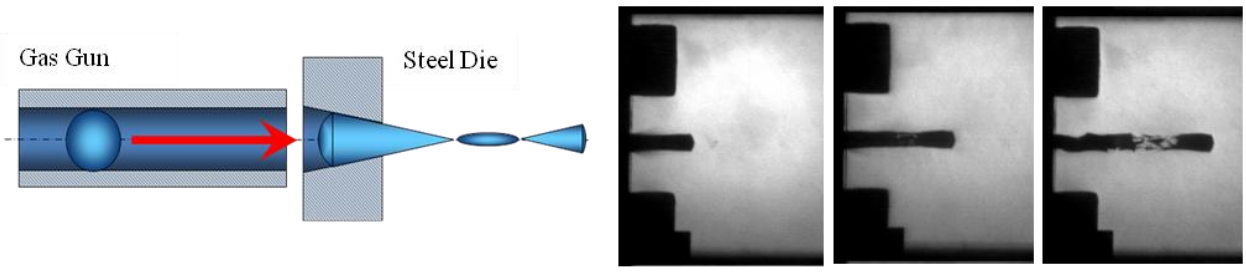

(a) **(b)**

Figure 4. (a) Schematic of the Dyn-Ten-Ext experiment and (b) sequenced high-speed video frames of the sample event.

The Taylor cylinder impact experiments were conducted at the MIT Institute for Soldier Nanotechnologies' (ISN's) high strain rate laboratory under Contract No. DAAD-19-02-D0002 with the U.S. Army Research Office. A 12.7-mm diameter bore single-stage gas gun was used to perform the Taylor cylinder impact experiments, as shown in figure 5 (*10*, *11*). A double diaphragm assembly was burst using pressurized nitrogen gas. Typical impact velocities reached up to 300 m/s when the breech pressure was of the order of 70 bar. Experiments were performed using PC cylinders that were 12.67-mm diameter and either 25.4-mm or 76.2-mm length (L/D ratios of 2:1 and 6:1, respectively) at impact velocities varying from approximately180–280 m/s. The flats of the samples were polished prior to experiments. A hardened stainless steel tile 100 × 100 mm wide × 12.7 mm thick and machine-ground and lubricated, was mounted on a steel frame and acted as the rigid surface. Impact velocity was measured by triggering two parallel laser ribbons monitored with photodiodes. Impacted specimens were recovered after rebound and sectioned for final deformed geometry. A Cordin high-speed charge-coupled device camera with a Nikon 70–300 mm lens, capable of acquiring images at a frame rate of 2 million frames per second, was used to record the event (*10*, *11*). A machine-grade PC procured from GE Plastics was used for all the MIT Taylor cylinder impact experiments. Although the material was extruded, compression Kolsky bar experiments (approximately 4000/s) showed that the material was fairly isotropic and the dynamic response was identical to Lexan PC 9034 (*10*).

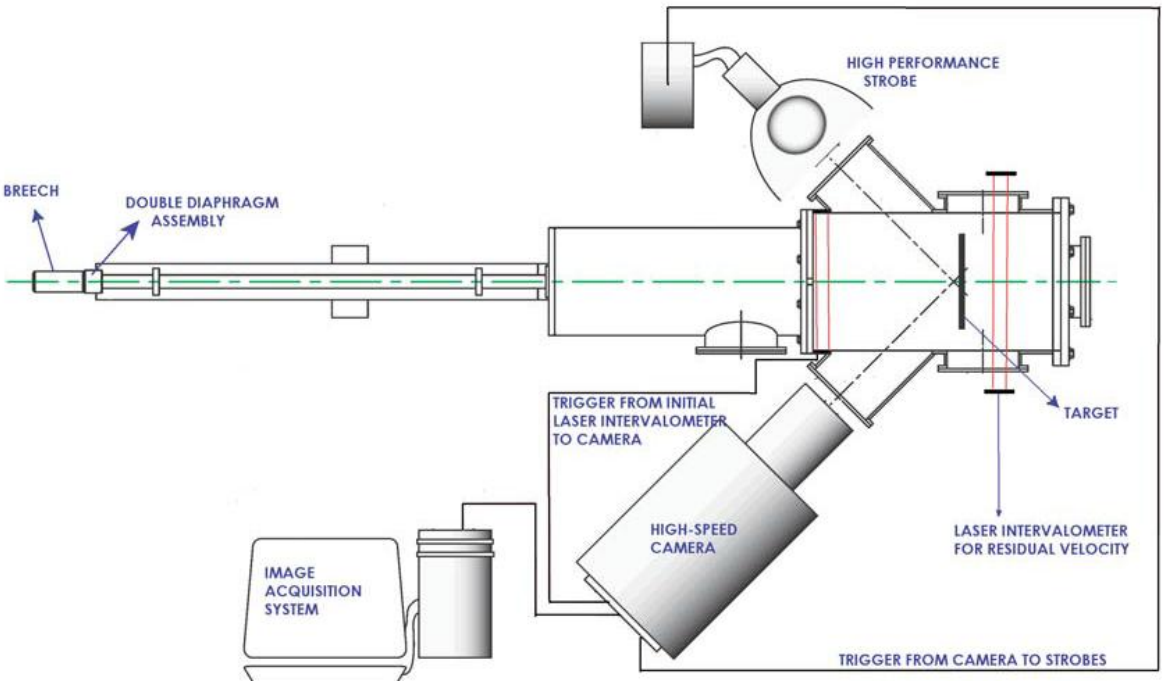

Figure 5. Schematic of the single stage gas gun used for the Taylor cylinder impact experiments at MIT ISN (*11*). The assembly shown is for an impact-penetration experiment using a finite thickness target.

Large sheets (1.22 × 2.44 m wide × 12.7 mm thick) of PC were obtained from Bayer Sheffield Plastics Makrolon. The sheets as received by ARL were extruded along the 2.44-m width. As previously mentioned, the Dyn-Ten-Ext apparatus in use at LANL is a slight modification to the Taylor cylinder impact configuration (*12*). The barrel has a smooth 7.62-mm (0.300-in) bore. The barrel discharges into a target chamber that is evacuated with a roughing pump to prevent interaction of the projectile with an atmosphere. While the chamber contains a polished hardened steel anvil during the Taylor cylinder impact experiment, for Dyn-Ten-Ext this is replaced with a catch tank loosely filled with cloth for soft recovery of any specimen fragments. The main data collected during a Dyn-Ten-Ext experiment consist of initial velocity from the bore prior to interaction with the die and high-speed multiframe photography of the extruded material for obtaining deformed shape and speed, which is then compared to numerical simulations to understand the material behavior during the experiment. The specimen's initial velocity is measured via two pressure transducers on the barrel near the target chamber and captured with an oscilloscope. The images of the extruded material are captured with an Imacon 200 or Shimadzu HPV2 framing camera (Hadland, Santa Cruz CA), typically with a 3–5 μs interframe time, and illumination is provided opposite the camera by a Powerlight 2599 flash lamp (Photogenic, Bartlett, IL). The velocity of extruded material is collected from the captured images and is calibrated with a transparent scale near the die exit.

The Dyn-Ten-Ext specimen geometry can be a sphere or a hemisphere-ended cylinder, both of which use a diameter and length of 7.60 mm; hemisphere-ended cylinders are shown in figure 6. The die uses a conical reducing section inclined 9° (half-angle) to the extrusion axis. The die exit diameter is specified depending on the desired draw ratio to be imposed prior to the onset of dynamic self-extrusion after the die exit. The nominal design of the die uses an exit diameter of 2.80 mm (0.110 in), which imposes an axial true strain $\varepsilon \sim 2$ at the die exit. All samples were machined at ARL and sent to LANL as part of a collaborative agreement between the author and G. T. Gray. The experiments were performed by J. Furmanski, C. Trujillo, D. Martinez, and CDT J. Tyler under the Joint Munitions Program, Technology Coordinating Group-I collaborative research efforts between DOE and U.S. Department of Defense agencies. To examine the influence of anisotropy due to rolling, hemisphere specimens were prepared in all three directions as shown in figure 5. Unfortunately, a faulty high-speed camera prevented completion of the parametric study but will be reported in the future upon completion. Results of the successful experiments provided ample data for the objectives of this report.

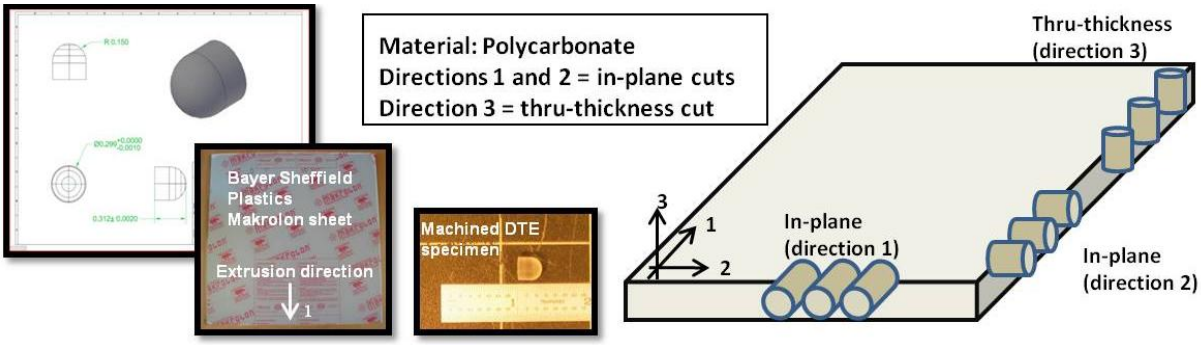

Figure 6. Hemishere-ended cylinder samples and directionality considered for polycarbonate as used for DynTen-Ext experiments.

3. Constitutive Model

It is well known that amorphous glassy polymers exhibit a strong dependence on strain rate and temperature as well as pressure dependence of modulus and strength. For numerous polymers, it has also been observed that there exists a transitional threshold in strain rate and temperature beyond which the strain rate sensitivity dramatically increases. The most widely accepted theory of rate dependent yield for glassy polymers connects macromolecular mechanisms of deformation resistance with macroscopic mechanical behavior (*13, 14*). The Eyring cooperative model assumed an existence of an internal stress as a structural parameter where defects are only inherited from thermal evolution. As an example, the glass transition temperature, T_g, is a useful parameter supporting this theory by differentiating the solid state from the rubbery state. Eyring considered plastic flow originated as a rate-activated process where molecules flowed from a particular potential well to another by overcoming an energy barrier (*13*). The shear strain rate, $\dot{\gamma}$, as a function of the shear stress, τ, in the polymer was written as,

$$\dot{\gamma} = \dot{\gamma}_0 \exp\left(\frac{\Delta H}{RT}\right) \sinh\left(\frac{\tau \emptyset}{RT}\right) \tag{1}$$

where ΔH is the activation energy; R is the universal gas constant; T is temperature; ϕ is the activation volume; and $\dot{\gamma}_0$ is a pre-exponential factor. In 1955, the Ree-Eyring model further accounted for microstructural mechanisms by relating molecular motions to yield behavior, denoted as α, β phases and written as,

$$\frac{\sigma_y}{T} = A_\alpha \left[\ln(2C_\alpha \dot{\varepsilon}) + \frac{Q_\alpha}{RT} \right] + A_\beta \sinh^{-1}\left[C_\beta \dot{\varepsilon} \exp\left(\frac{Q_\beta}{RT}\right) \right] \tag{2}$$

where σ_y is the yield stress under uniaxial loading; $\dot{\varepsilon}$ is the strain rate; Q_i ($i = \alpha,\beta$) are activation energies for the two processes; and A_i and C_i are activation parameters (*14, 15*). For PC, the results of Dynamic Mechanical Analysis (DMA) plotting storage and loss moduli as functions of

temperature are shown in figure 7. Mulliken and Boyce (*16*) developed an expression describing the α mechanism for low strain rates and high temperatures, whereas the β mechanism refers to high strain rates and low temperatures. Taken together, the α and β phases will be denoted as segment A.

To determine strain rate sensitivity of the yield stress, a set of quasi-static Instron and dynamic Kolsky bar compression experiments were conducted for PC, as shown in figure 8 (a). Rate sensitivity was then reduced from the observations in figure 8 (b) as two distinct regions for increasing flow stress with strain rate. It was then determined that this transition (approximately1500/s) was in close agreement with the transition observed from DMA data (*16*). This insight of rate-sensitive transitions formed the foundation of the M-B constitutive model for amorphous polymers.

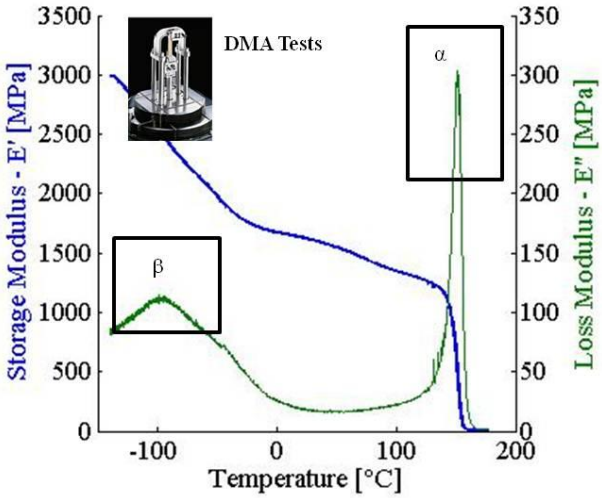

Figure 7. Storage and loss tangent moduli for PC; DMA experiments performed at 1 Hz and shift at 100 Hz showing the α and β transition regions using the Deconstruct-Shift-Reconstruct analytical method (*16*).

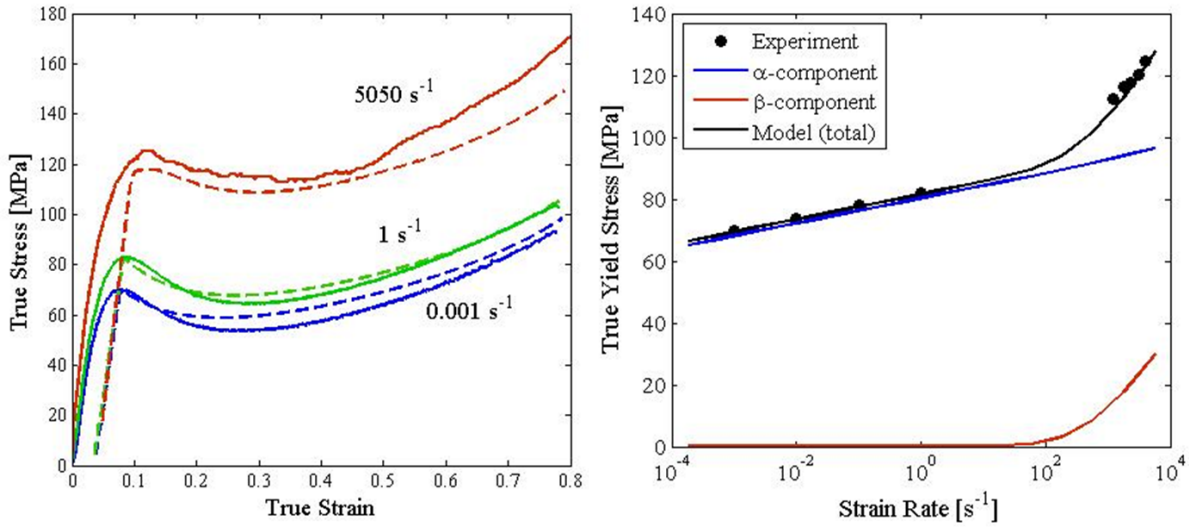

(a) **(b)**

Figure 8. (a) Observed uniaxial compression response of PC over a range of strain rates performed at room temperature; (b) strain rate sensitivity of flow stress (*16*).

The M-B model is built on the foundation of the Ree-Eyring and Eyring cooperative model as previously described, and is an extension of the Arruda-Boyce model by capturing glassy polymer behavior at high rates of deformation (*16*). Similar to a mixture theory, material response in the M-B model are described using three mechanisms (two segment A's and a segment B) acting in parallel and simultaneously co-existing at a material point, as shown in figure 9. The deformation is decomposed into elastic and plastic parts for each phase and each phase sees the same total deformation. The constitutive equations do not assume a yield surface; therefore, plasticity occurs at all times during deformation. The total Cauchy stress tensor, **σ,** at a material point is written as the sum,

$$\boldsymbol{\sigma} = \boldsymbol{\sigma}_B + \boldsymbol{\sigma}_\alpha + \boldsymbol{\sigma}_\beta \tag{3}$$

where $\boldsymbol{\sigma}_\alpha$ and $\boldsymbol{\sigma}_\beta$ are the Cauchy stress tensors for the α and β phases. Referring back to figure 9, $\boldsymbol{\sigma}_B$, the segment B mechanism represents macromolecular resistance to chain stretching and alignment; thus, it is a strain hardening term with no dependence on strain rate and temperature.

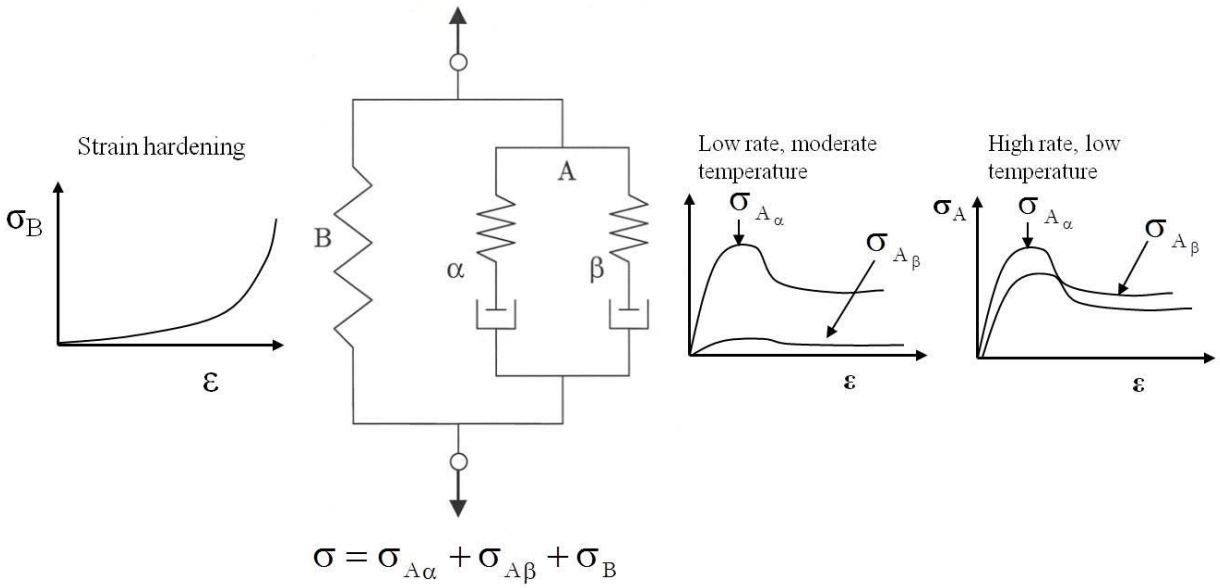

Figure 9. One-dimensional (1-D) depiction of the M-B constitutive model (*16*). The spring in segment B is a strain hardening Langevin (nonlinear) spring representing chain stretching and alignment; the springs in segment A are rate- and temperature-dependent elastic (linear) springs and the dashpots represent rate-, temperature-, and pressure-dependent viscoplastic terms for intermolecular resistance.

The stress in the nonlinear hardening segment B, $\boldsymbol{\sigma}_B$, uses the original description by Arruda and Boyce (*17*) and written as,

$$\boldsymbol{\sigma}_B = \frac{C_R}{3}\frac{\sqrt{N_l}}{\lambda^p_{chain}}\mathcal{L}^{-1}\left(\frac{\lambda^p_{chain}}{\sqrt{N_l}}\right)\overline{\boldsymbol{B}}'_B \tag{4}$$

where $\lambda^p_{chain} = \sqrt{tr\left(\overline{\boldsymbol{B}}'_B\right)}/3$ measures chain stretch in an 8-chain network; $\mathcal{L}$ is the Langevin function defined by $\mathcal{L}(\beta) = \coth\beta - \frac{1}{\beta}$; $\overline{\boldsymbol{B}}'_B$ is the deviatoric part of the isochoric left Cauchy-Green tensor, $\overline{\boldsymbol{B}}_{\boldsymbol{B}} = (\det\boldsymbol{F})^{-2/3}\boldsymbol{F}\boldsymbol{F}^{\mathrm{T}}$; N_l is the limiting chain stretch; and $C_R = nkT$ is the rubbery modulus (where n is the number of chains per unit volume, k is Boltzmann's constant, and T is the absolute temperature).

Segment A represents the intermolecular resistance to chain-segment rotation; thus, the two parallel subsegments are thermal softening terms that are strain rate and temperature dependent. For PC, the α-subsegment represents rotations of the entire monomer chain and the β-subsegment represents rotations of the phenyl group. The viscoplastic behavior connecting stress to effective plastic strain rate for each intermolecular resistance subsegment can be written as,

$$\dot{\gamma}^p_i = \dot{\gamma}^p_{0,i}\, exp\left[\frac{-\Delta H_i}{RT}\left(1 - \frac{\tau_i}{t_i S_i + \alpha_i\, p}\right)\right] \tag{5}$$

where i=α, β for the two component phases, S_i is the athermal shear strength (related to shear modulus and Poisson ratio), α_i a pressure coefficient, and $p = -\sigma_{ii}/3$ is the pressure. Note the similarity to equation 1. Also, the viscoelastic behavior as observed from the DMA experiments is incorporated into the M-B model through the shear modulus in segment A. The internal history variable t_i in equation 5 accounts for strain softening in glassy polymers. The evolution equation for the internal variables is written as,

$$\dot{t}_i = \frac{h_i}{S_i^0}\left(1 - \frac{t_i}{t_i^{ss}}\right)\dot{\gamma}_i^p \tag{6}$$

and the shear strength is,

$$S_i = \frac{0.077\,\mu_i}{1-\upsilon_i} \tag{7}$$

where h_i are softening slopes, S_i^0 are the "preferred state" of the shear strengths, t_i^{ss} are material parameters used to limit softening due to plastic work, μ_i are shear moduli as functions of temperature, and strain rate and υ_i are the Poissons ratios for each phase, which are assumed to be constant. The effective plastic strain rate, $\dot{\gamma}_i^p$, as given by equation 5 is equal to zero when deformations are elastic only. Also, t_i^{ss} is a steady state value for τ_i, which sets a lower limit on strength.

The M-B constitutive equation as described using equations 5–7 include amendments by Varghese and Batra (*18*) to account for the temperature rise due to 100% plastic work-to-heat conversion. In 2012, the M-B model was implemented by R. Becker, ARL, into the LLNL hydrocode suite ALE3D (*3*). The implementation followed the kinematic approach used by Varghese and Batra (*18*); however, some modifications were required. Specifically, Becker did not use multiplicative decomposition of the deformation gradient into elastic and plastic parts but used an updated Lagrangian form that would be less problematic with advection. Also, the initialization of the temperature and rate dependent shear modulus was set using prevailing conditions instead of initialization to the anticipated experimental conditions used by Varghese and Batra. Finally, the pressure-volume response is given by a nonlinear equation-of-state which also depends on deformation energy, whereas the earlier work used a constant bulk modulus. Further details on the implementation of M-B into ALE3D and other DOE hydrocodes will be made available in a future report.

Model parameters for the M-B model were optimally fit using two types of experiments: DMA experiments for the viscoelastic behavior of the loss storage modulus and quasi-static/dynamic compression experiments for rate sensitive viscoplastic response. The original parameter fits for PC obtained by Mulliken and Boyce (*16*) considered only isothermal conditions and are shown in figure 8 (a). The contribution of the β-component is clearly seen in figure 8 (b) with the ability to describe the increase in flow stress at high strain rates. Varghese and Batra (*18*) assumed that all the energy dissipated due to plastic work was converted into heat (adiabatic heating) and re-fit the model by adjusting the chain stretch coefficients. They also split the original internal variable

S_i into two components as now given in equation 5; one accounting for the rate and temperature dependent modulus and the other a pure evolution, as written in equations 6 and 7, respectively. As a result, they obtained another set of model parameters for PC that considered the temperature rise due to plastic deformation and compared it with the isothermal parameters, shown in figure 10.

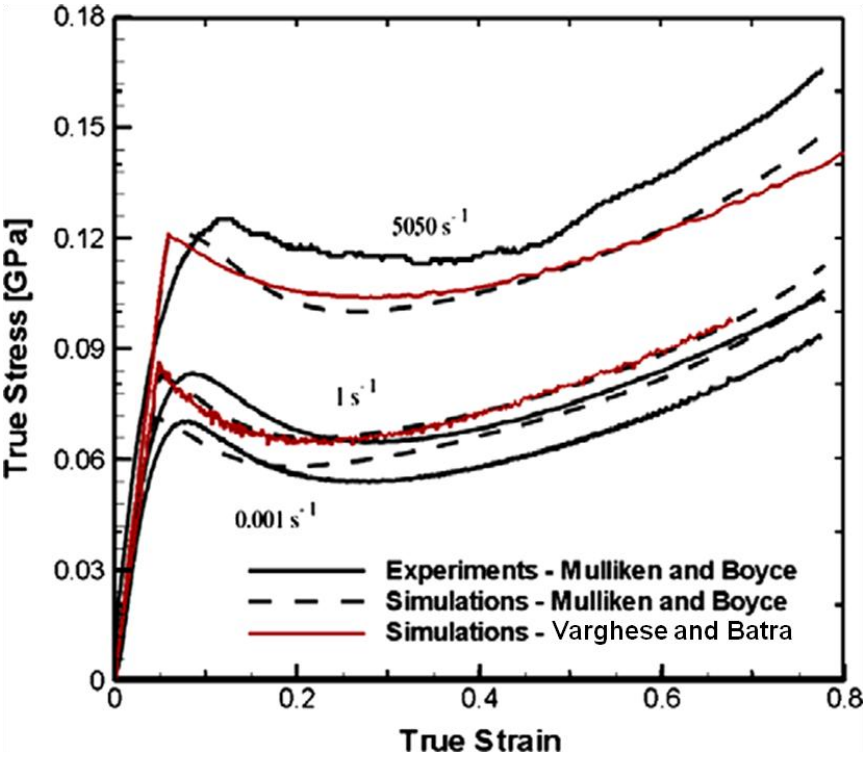

Figure 10. Comparison of PC material response in uniaxial compression using the M-B model for parameters obtained assuming isothermal conditions (labeled Mulliken and Boyce in plot) and modified parameters for plastic work (labeled Varghese and Batra in plot) (*18*).

4. Numerical Considerations

A performance evaluation using all three model parameter sets discussed in the previous section was completed numerically for dynamic compression and dynamic tension loading conditions. All computational modeling was performed on a twelve-processor Linux computer using the hydrocode ALE3D (*3*), developed at LLNL. The boundary conditions for the Taylor cylinder impact experiments are shown in figure 11. An ALE3D input file was created describing the geometry, initial conditions, boundary conditions, and material response models. Analyses were conducted using a two-dimensional axisymmetric geometry. Symmetry along the centerline was described by constraining the centerline nodes with no displacement in the radial direction. The

boundary of the cylinder was Lagrangian, and the interior nodes were free to advect. Also, the rigid wall was described by constraining the boundary nodes along the impacted end to not cross the impact plane. This input allowed the cylinder to rebound in the negative axial direction after the reflected tensile wave arrived at the impacted end and effectively stop any further loading due to impact.

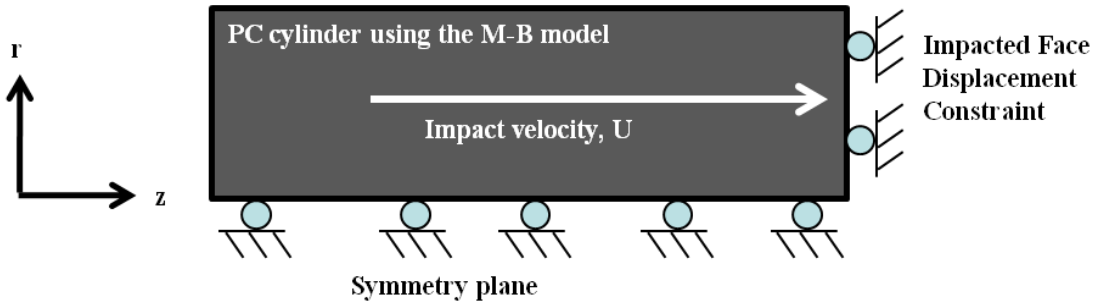

Figure 11. Schematic illustrating the reference configuration, initial conditions, and boundary conditions used for the ALE3D Taylor cylinder impact simulations.

The computational domain for the Dyn-Ten-Ext experiments is shown in figure 12. The simulation was run in an Eulerian mode with a fixed mesh. Axisymmetry along the centerline was described by constraining the centerline nodes with no displacement in the radial direction. A frictionless surface was used to describe the rigid extruding die. The options used in these Eulerian simulations do not allow the material to separate from the die. This drives the timestep down and eventually stops problem execution during elastic recoil. The issue during rebound can be avoided by alternatively applying a slide surface that detaches from the deforming cylinder. Results for model performance will only be discussed as the cylinder begins to exit the die and before the stress on the die surface becomes tensile.

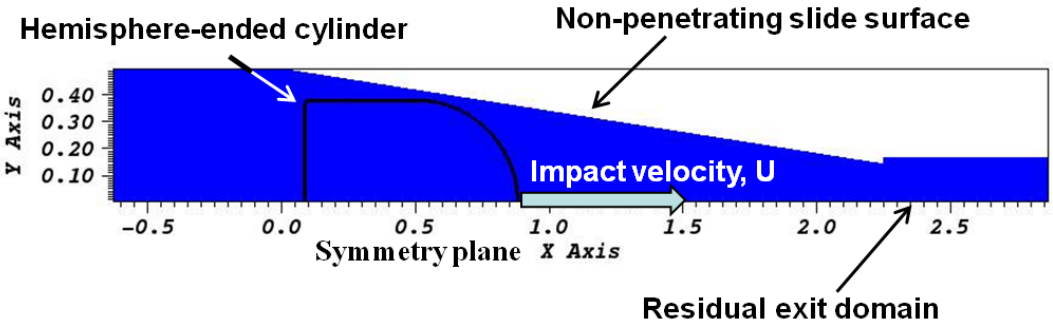

Figure 12. Schematic illustrating the reference configuration, initial conditions, and boundary conditions used for the ALE3D Dyn-Ten-Ext simulations.

For both numerical simulations, the initial velocity of the projectile was the observed impact velocity. The governing equations for spatial and temporal deformation of the cylinder were solved using an Eulerian formulation. Elements were approximately square with a mesh density of approximately 0.2 mm/element in the r- and z-directions. The consistent units used for all numerical simulations were cm, g, μs, Mbar, and K.

ALE3D is a large deformation continuum mechanics code that contains a material strength formulation. Typically, the constitutive formulation can be subdivided into five parts: (1) a stress/strain relationship for elastic material response, (2) a yield surface that specifies the multiaxial stress state corresponding to the start of plastic flow, (3) a flow rule that describes plastic behavior after yielding by relating strain increments to stress increments, (4) a consistency statement that constrains the stress state to remain on the yield surface during plastic flow, and (5) a hardening rule that describes the evolution of the flow strength during plastic deformation. The constitutive relation or flow rule physically describes material response by relating stresses to deformations. The finite element framework mathematically connects kinematics and field equations with boundary conditions. Most generally, a constitutive relation for the material flow strength, $\bar{\sigma}$, can be written as some function,

$$\bar{\sigma} = \tilde{\sigma}\,(\varepsilon, \dot{\varepsilon}, T, p, \beta) \tag{8}$$

ε is the plastic strain in the current configuration, $\dot{\varepsilon}$ is the plastic strain rate, T, the temperature, p, the pressure, and β is some internal state variable. Most empirical constitutive models (e.g., Johnson-Cook strength model) are constructed on macroscopic material response experiments and do not track a state variable; they are written as,

$$\sigma = \sigma\,(\varepsilon, \dot{\varepsilon}, T, p) \tag{9}$$

Several phenomenological constitutive models including an M-B attempt to provide a better representation of the underlying physics using an internal state variable β to describe structure evolution. The flow stress can now be written as,

$$\bar{\sigma} = \tilde{\sigma}\,(\dot{\varepsilon}, T, p, \beta) \tag{10}$$

5. Results

A parameter sensitivity analysis was performed with the M-B model at extreme loading environments that approach the ballistic regime. The two experiments previously described provide "isolated" loading conditions of dynamic compression and dynamic tension. The purpose of this numerical analysis was not to match or validate model parameters to the observed. Instead, the given model parameters where used as a baseline for a given loading condition, and particular mechanisms were carefully disabled then compared to the baseline case. This is an example of one method required for sensitivity analysis. Another would require

changing the functional form of physical descriptions in model and comparing to a baseline ballistic impact experiment. The method of changing mathematical forms will be considered in future research endeavors.

The M-B model in its most general form describes three intermolecular activation processes that simultaneously influence material deformation at the continuum level. The first describes chain stretch as related to strain hardening and the others describe strain softening for low strain rates, high temperatures and high strain rates, low temperatures, respectively. This was described mathematically using the 1-D spring-dashpot system, as shown in figure 9, using springs for the nonlinear elastic behavior and dashpots for viscoplasticity. A model parameter sensitivity analysis was performed for a better understanding on the influence of these simultaneously competing mechanisms subjected at high rate loading conditions. The dependence of flow strength on strain rate sensitivity and pressure was examined as function of these competing deformation mechanisms.

Specifically, three mechanisms were individually turned off or minimized in this parametric study:

(1) No low strain rate activation mechanism; disabled dashpot-α of subsegment A.

(2) No high strain rate activation mechanism; disabled dashpot-β of subsegment A.

(3) No pressure dependence in the chain rotation activation mechanism; disabled pressure in the effective plastic strain rates terms of segment A.

Values of M-B material parameters for PC are given in table 1 and subdivided according to the 1-D spring-dashpot system, as previously described. To obtain M-B model parameters requires reduced DMA data for defining the elastic springs. These are piecewise cubic splines that are not given in table 1 but are available in the ALE3D implementation. A set of uniaxial compression experiments (quasi-static and dynamic) are required for a piecewise breakdown of yield behavior as defined using the viscoplastic dashpots. Note that the values listed in table 1 were obtained by Varghese and Batra (*18*) and accounted for the temperature rise from plastic work to heat (i.e., locally adiabatic deformations) as encountered during high rate loading events.

Table 1. M-B model parameters for PC (*18*).

MB Parameter	Parameter Description	Nominal Value
Rate-dependent elastic springs		
$\mu_i(T,\dot{\epsilon})\ for\ i=\alpha,\beta$	Process-specific shear moduli as functions of temperature and strain rate	Obtained from DMA data
$\kappa_i(T,\dot{\epsilon})\ for\ i=\alpha,\beta$	Process-specific bulk moduli as functions of temperature and strain rate	Obtained from DMA data
Viscoplastic dashpots		
$\dot{\gamma}_{0,i}^{p}\ for\ i=\alpha,\beta$	Pre-exponential factors	2.94e+16 , 3.39e+05
$\Delta H_i\ for\ i=\alpha,\beta$	Activation energies	3.744e-18, 3.769e-20
$\alpha_i^{p}\ for\ i=\alpha,\beta$	Pressure coefficients	0.168, 0.245
$h_i\ for\ i=\alpha,\beta$	Softening slopes	125 MPa, 400 MPa
$t_i^{ss}\ for\ i=\alpha,\beta$	Preferred states of strain softening; added by (*18*)	0.33, 2.00
Langevin springs		
C_R at 300K	Rubbery modulus	35 MPa
$\sqrt{N_l}$	Limiting chain extensibility	3.5

5.1 Dynamic Compression

Taylor cylinder impact experiments were conducted using PC cylinders with a 12.7-mm diameter and 76.2-mm length at normal impact velocities ranging from 180 to 200 m/s. Results are numerically predicted for the representative case with no fracture (only deformation) at 187 m/s (*18*).

High-speed video frames of the impact event are shown in figure 13. After the PC cylinder has made contact with the rigid anvil (frame 2 in figure 13), the deformation at the impacted end flows radially and results in the formation of a mushroom head (frames 3–5 in figure 13). At 72 μs (frame 6 in figure 13), radial barreling forms above the mushroom head at approximately 20% above the foot of the original length. This spreading of the deformation zone is primarily due to strain hardening from chain alignment. The cylinder continues to deform until it rebounds at approximately 198 μs (frame 11 in figure 13). It is during and after this rebound stage that the cylinder displays elastic recovery until the loading event stops at 230 μs. Measurements of the recovered specimen revealed plastic radial expansion over approximately one-half the length (*11*).

Considering the differences in implementation and parameters, numerical simulations of the Taylor cylinder impact experiment using the Varghese, Batra, Becker (VBB) model parameters favorably agreed with the original M-B model results, as shown in figures 14, 15, 16 (a), and 16 (b). Figure 14 shows the evolution of axial stress, figure 15 plastic strain rate, and figure 16 pressure. The montage of predicted shapes matched well with the observed including the mushroomed head, radial barreling, and elastic recoil. Subtle differences compared with the predictions using the original M-B model parameters are attributed to the following features using the VBB model parameters:

(1) Temperature rise from plastic work-to-heat conversion (original M-B parameters considered only isothermal deformations).

(2) Equation-of-state used with VBB parameters in ALE3D where the shear modulus is split into two parts (Young's modulus and Poisson's ratio used to obtain a shear modulus with the original M-B parameters).

(3) Modifications to ALE3D VBB model parameters for segment A terms.

(4) Modulus and history variables initialized to predefined strain rate in M-B model.

These differences are expected to be more pronounced at higher strain rates and larger deformations.

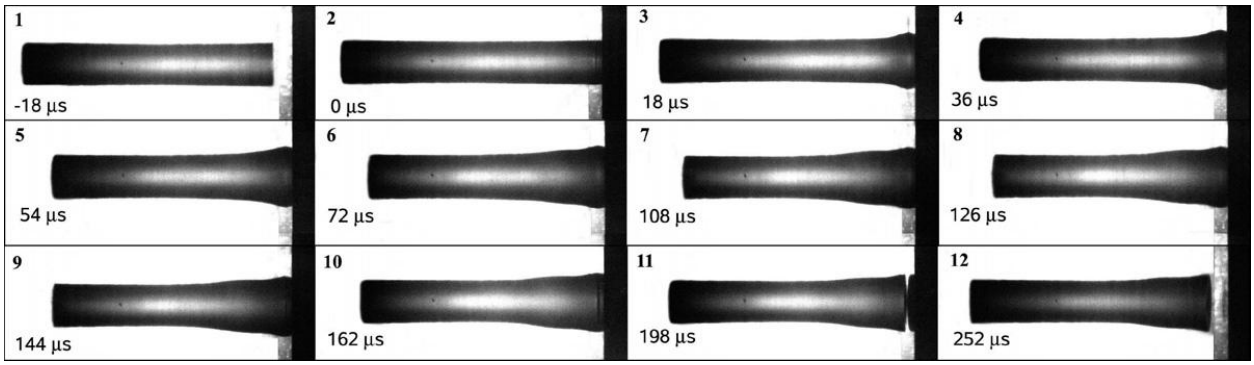

Figure 13. High-speed video frames recorded at various stages during a Taylor cylinder impact experiment on a 76.2-mm PC rod at 187 m/s. Note elastic recovery after 100 μs and rebound (detachment from rigid surface) at 198 μs *(11)*.

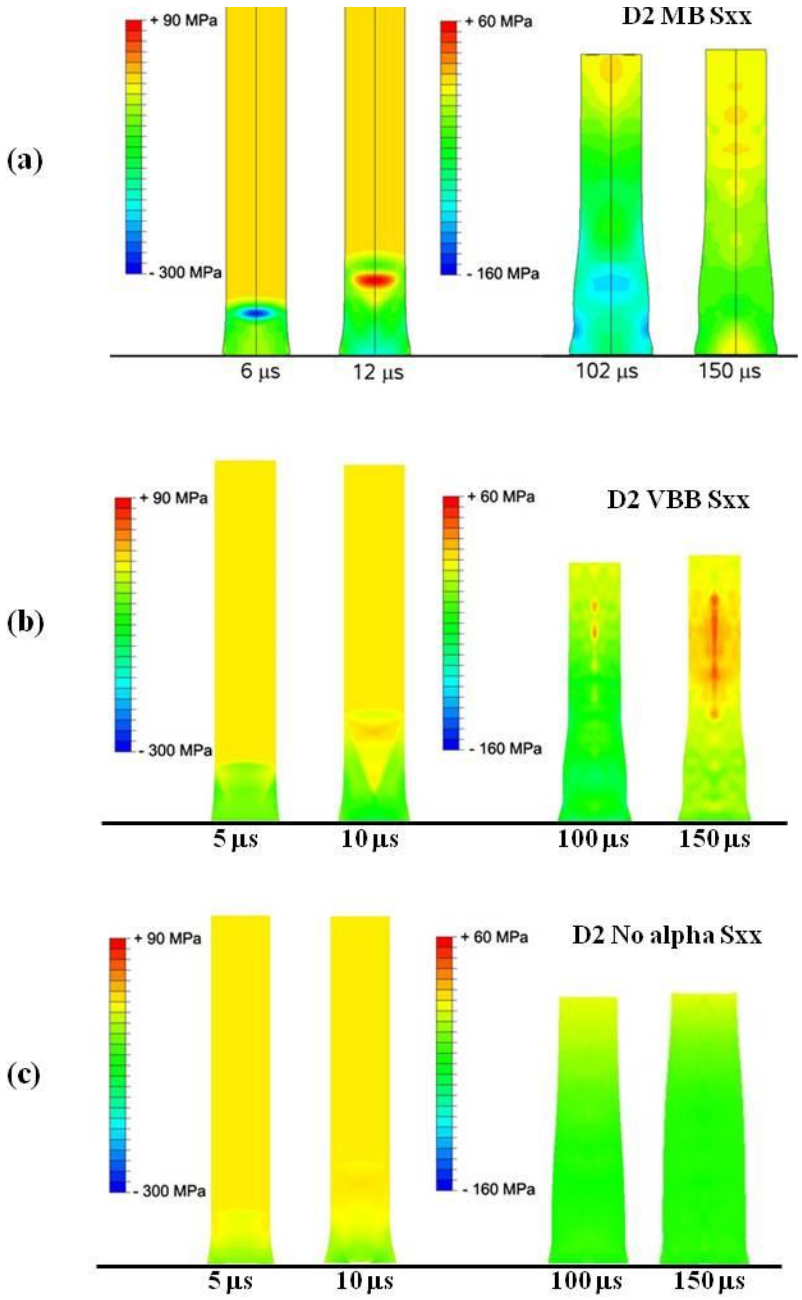

Figure 14. Parameter sensitivity showing numerical contours of axial stress using the M-B model for a Taylor cylinder impact experiment at a striking velocity of 187 m/s (labeled D2) at sequential times after rigid impact. (a) Full original parameters used in M-B courtesy of *(11)*, (b) full VBB parameters used in M-B, (c) VBB parameters used in M-B with the viscoplastic α phase disabled, (d) VBB parameters used in M-B with the viscoplastic β phase disabled, (e) VBB parameters used in M-B with pressure dependence of strength disabled, (f) comparison of temperature rise due to plastic work-to-heat conversion near end of impact event using (i) full VBB parameters in M-B, (ii) α phase disabled, (iii) β phase disabled, (iv) pressure dependence disabled.

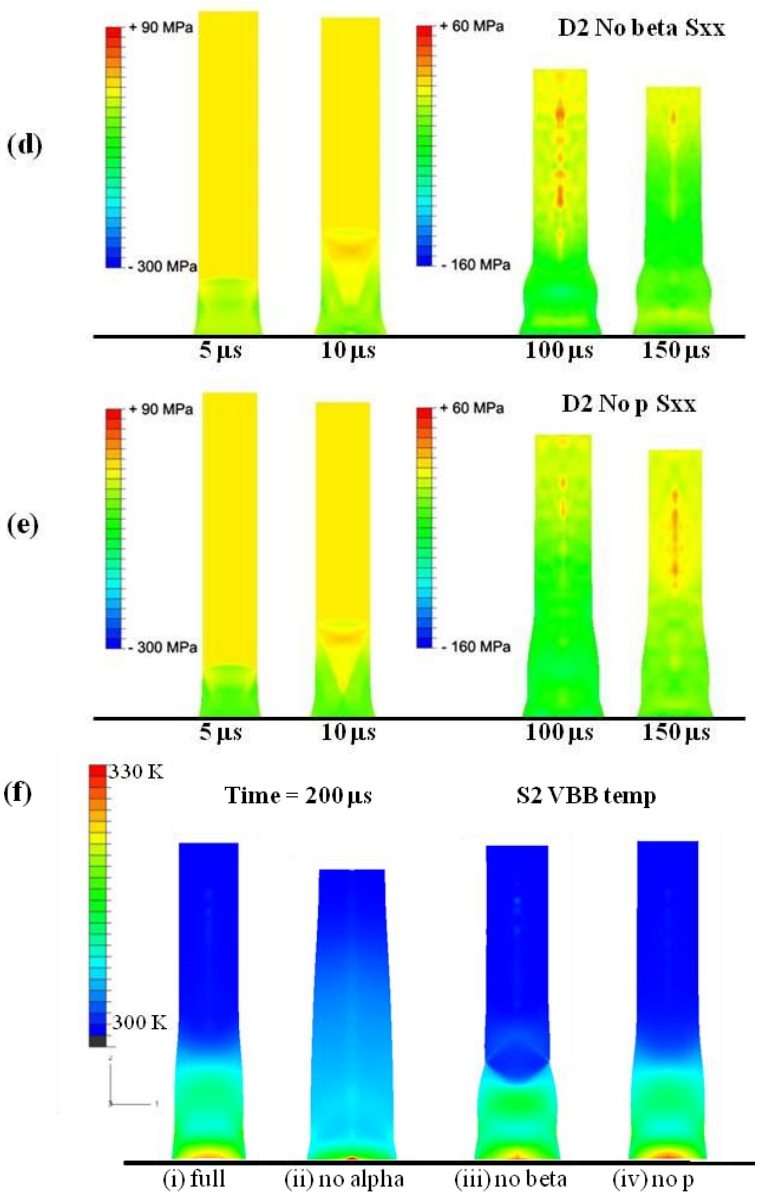

Figure 14. Parameter sensitivity showing numerical contours of axial stress using the M-B model for a Taylor cylinder impact experiment at a striking velocity of 187 m/s (labeled D2) at sequential times after rigid impact. (a) Full original parameters used in M-B courtesy of *(11)*, (b) full VBB parameters used in M-B, (c) VBB parameters used in M-B with the viscoplastic α phase disabled, (d) VBB parameters used in M-B with the viscoplastic β phase disabled, (e) VBB parameters used in M-B with pressure dependence of strength disabled, (f) comparison of temperature rise due plastic work-to-heat conversion near end of impact event using (i) full VBB parameters in M-B, (ii) α phase disabled, (iii) β phase disabled, (iv) pressure dependence disabled (continued).

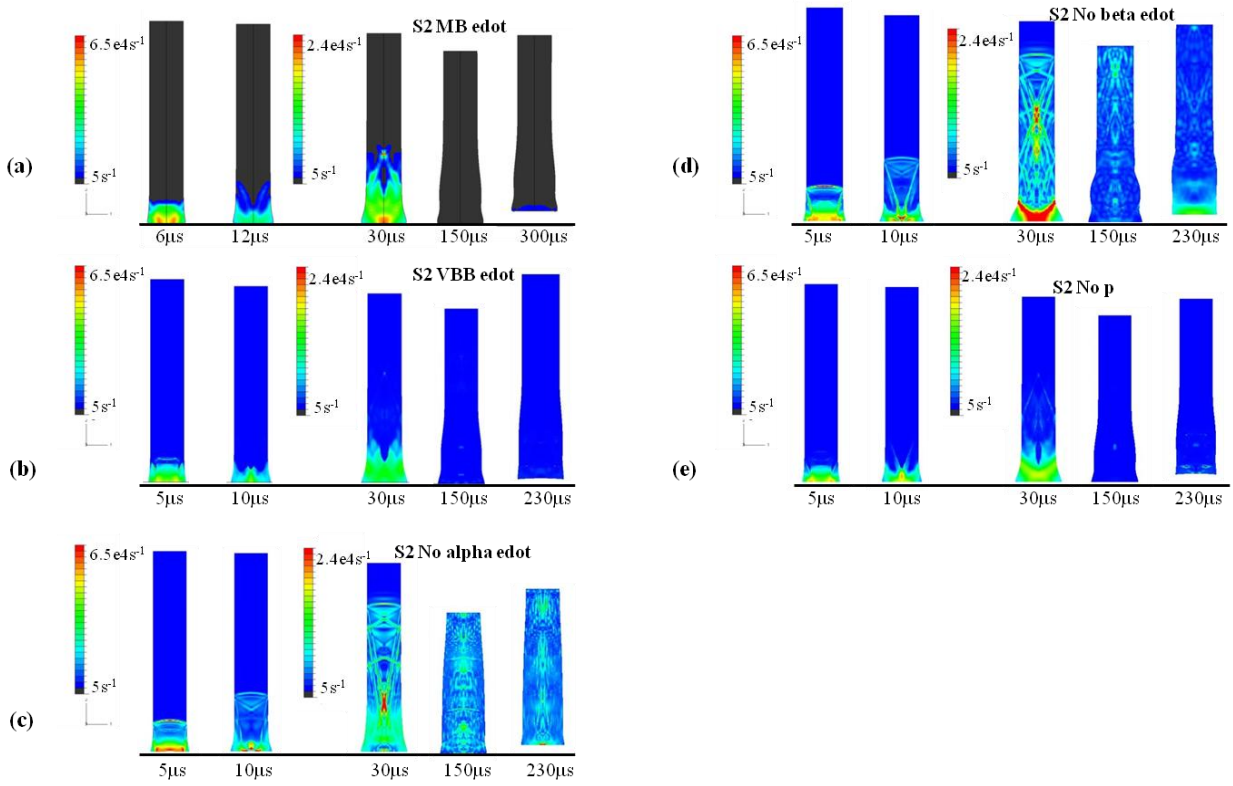

Figure 15. Parameter sensitivity showing numerical contours of strain rate using the M-B model for a Taylor cylinder impact experiment at a striking velocity of 187 m/s (labeled S2) at sequential times after rigid impact. (a) Full original parameters used in M-B courtesy of *(11)*, (b) full VBB parameters used in M-B, (c) VBB parameters used in M-B with the viscoplastic α phase disabled, (d) VBB parameters used in M-B with the viscoplastic β phase disabled, and (e) VBB parameters used in M-B with pressure dependence of strength disabled.

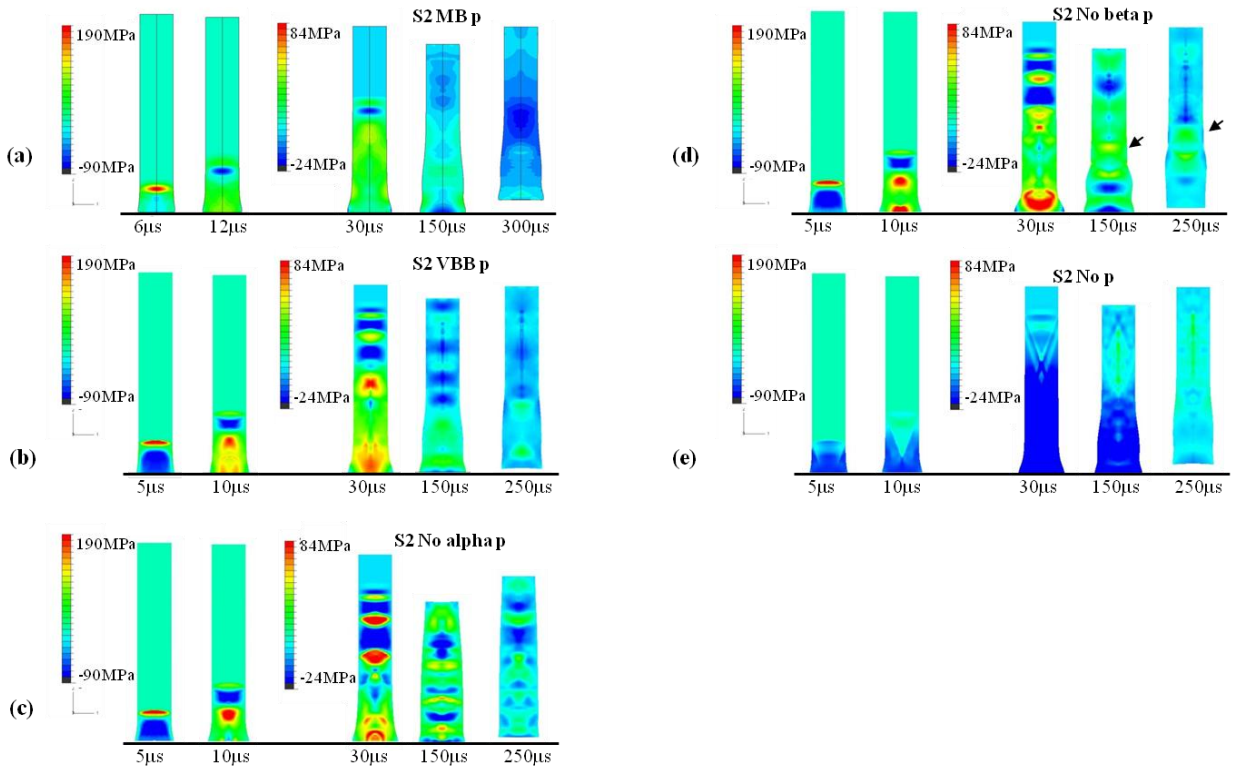

Figure 16. Parameter sensitivity showing pressure contours using the M-B model for a Taylor cylinder impact experiment at a striking velocity of 187 m/s (labeled S2) at sequential times after rigid impact. (a) Full original parameters used in M-B courtesy of *(11)*, (b) full VBB parameters used in M-B, (c) VBB parameters used in M-B with the viscoplastic α phase disabled, (d) VBB parameters used in M-B with the viscoplastic β phase disabled, and (e) VBB parameters used in M-B with pressure dependence of strength disabled.

The numerical results provided insight into the evolving stress state within the material as related to deformation. High strain rates and compressive stress (on order of 5e+04/s and 400 MPa) are induced in PC immediately after impact within the first 10 μs of the event (figures 14 [b] and 15 [b]). Afterwards, the magnitude of stress decreases until the transient nature of stress begins to stabilize (after 30 μs) as the compressive front travels to the rear of the cylinder (figures 14 [b] and 15 [(b]). The elastic compressive wave front reached the rear end at approximately 45 μs and is followed by a slower moving plastic deformation wave front. It is the plastic front that induced the resulting mushroomed head on the impacted (foot) end. Upon reaching the non-impacted end of the cylinder, the elastic compressive front reflects as a tensile front to maintain the zero stress state on the free surface. Afterwards, the reflected elastic tensile front interacts with the plastic front as seen by the profiles at 100 μs and 150 μs of figure 14 (b). The cylinder rebounded at approximately 195 μs followed by significant elastic recoil, as seen by comparing the deformed profiles for 150 μs and 230 μs of figure 15 (b).

For the same instant of time, regions of high strain rate are directly related to zones of high plastic deformation. Peak strain rates of about 4e+04/s were achieved between 5 and 30 μs after impact, as shown in figure 15 (a) and (b) at 5 μs and 30 μs, and subsequently diminish after 45 μs, as shown in figure 15 (a) and (b) at 150 μs. Most of the plastic deformation including mushrooming occurred in the initial 40 μs of the impact event and radial barreling occurred in the range of 50–100 μs. Negligible plastic deformation was predicted after rebound from the rigid surface. A review of the results shown in figures 15–17 (a) and (b) clearly indicated that the high rate dynamic loading conditions subjected PC to high-deformation gradients during a Taylor cylinder impact experiment.

The parameter sensitivity analysis examined the influence of the viscoplastic dashpots on the deformed state of the PC cylinder. Recall the rate dependence of the dashpots on flow strength, as shown in figure 8 (b). By disabling the α-dashpot, more strain hardening spread axially within the cylinder; the zone of moderate strain rate expanded at early stages (before 40 μs) and resulted in a larger barreled zone, as shown by comparing figures 15, 16, and 17 (c) with (b). By disabling the high-rate β dashpot and maintaining the low-rate α dashpot, more localized high strain rates were generated above the mushroomed head and resulted in wider radial barreling between 30 and 100 μs, as shown by comparing figures 15, 16, and 17 (d) with (b) and (c). Finally, disabling pressure dependence in both viscoplastic α and β dashpots resulted in negligible differences as compared with full VBB parameter set for the M-B model, as shown by comparing figures 15, 16, and 17 (e) with (b). The pressure dependent results are not surprising since hydrostatic pressures generated during Taylor cylinder impact are small when compared with axial stress. This is not expected to be the case for more extreme ballistic environments where pressure dependence of flow strength has a greater influence on material deformation.

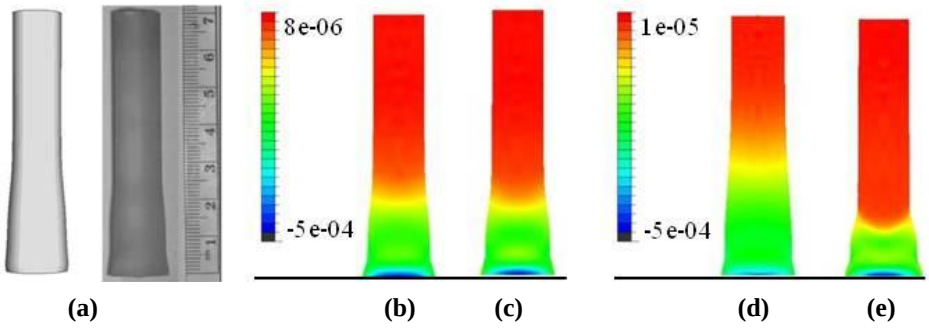

Figure 17. Comparison of strain hardening due to chain stretching for PC striking a rigid anvil at 187 m/s. Deformed shape and contours shown at the end of impact event for (a) experiment courtesy of *(11)*, (b) full VBB parameters, (c) VBB parameters with pressure dependence of strength disabled, (d) VBB parameters used in M-B with the viscoplastic α phase disabled, and (e) VBB parameters used in M-B with the viscoplastic β phase disabled.

Figure 17 shows the final deformed lengths of the full VBB parameter M-B model compared favorably with observed. Additionally for figure 17 (b–e), chain stretch in the deformed cylinder as calculated from the Langevin spring segment B is shown for the three parameter sensitivity sets. There are negligible differences in hardening by disabling pressure dependence at these strain rates, as seen by comparing figure 17 (c) with (b). By disabling the low-rate α dashpot, an increased zone of chain alignment indicated that large deformation gradients existed along the axial direction that resulted with increased strain hardening within the cylinder as shown in figure 17 (d). By disabling the high-rate β dashpot and maintaining the low-rate α dashpot, resistance to high-rate deformation decreased resulting in a softer or more rubbery-like material that barreled in the radial direction, as shown in figure 17 (e).

Finally, an important advantage for using the Varghese and Batra (*18*) modifications with hydrocode adjustments by Becker, is shown in figure 14 (f) for the temperature rise in the cylinder. The cylinder temperature increase an amount of 30 K by the end of the impact event using the modifications for 100% plastic work-to-heat conversion. This increase in temperature was not accounted for in the original M-B implementation (considered only isothermal deformations). Therefore, to model ballistic events for amorphous polymers at extreme loading conditions it is strongly recommended to use the modified M-B model with VBB parameters as given in table 1.

5.2 Dynamic Tension

A range of experimental results was obtained as the striking velocity of the .30-caliber specimen was increased, progressing from intact arrest with incipient cracking and void nucleation, to terminal damage progression through a circumferential tearing and central void progression process. Although damage and failure of PC is not considered for evaluating parameter performance in the M-B model, the Dyn-Ten-Ext results merit a brief sidebar on this topic.

The experiments performed to date captured damage evolution within the specimen subjected to extreme tensile conditions and also revealed that two separate mechanisms (or at least pathways) of damage were active during deformation. At lower velocities, the specimen did not extrude but was observed to form a neck at the hemisphere tip, as shown in figure 18 (a). Behind this neck, spherical voids nucleated in a number of cases. Further behind the neck, circumferential fracture was observed to initiate. These arrested damage features are believed to dominate failure and resulted in rupture of the specimen under more extreme loading conditions, as shown in figure 18 (b). Alternative experiments using notched specimens observed PC cavitations and failure in a brittle manner when subjected to moderate strain rates and experiencing tensile pressures with magnitude on the order of 80 MPa (*19, 20, 21*).

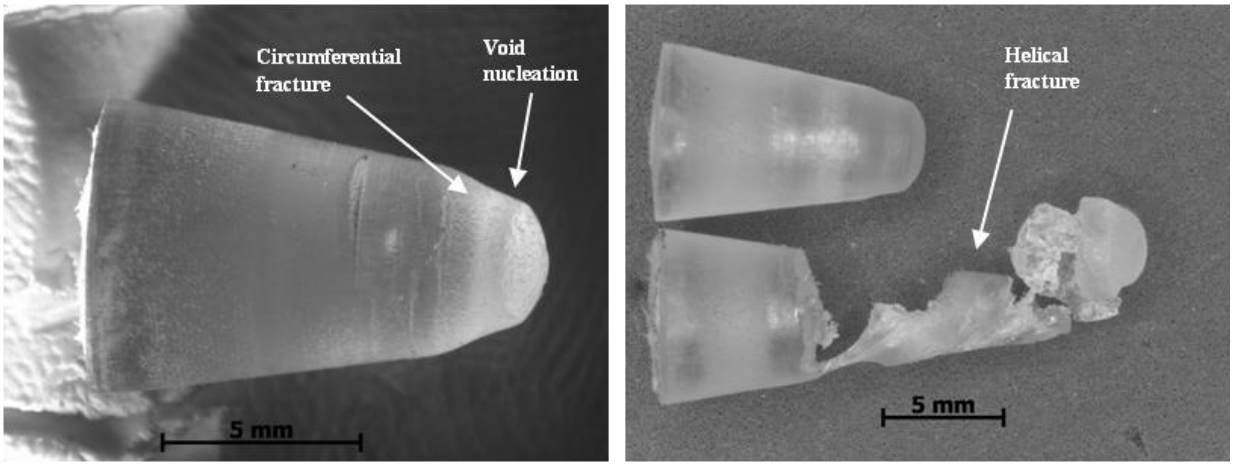

Figure 18. Recovered .30-caliber specimens from Dyn-Ten-Ext experiments for PC. (a) Arrested intact specimen from low velocity impact (less than 350 m/s), showing necking, void nucleation behind the neck, and circumferential fracture behind the void. (b) Comparison of arrested intact specimen and failed specimen (upper is low velocity, lower is high velocity), where central voiding and peripheral fracture have proceeded nearly to complete failure. There is a small ligament of unfractured material remaining in the failed part.

High-speed video frames of the failure process during extrusion experiments revealed the dynamics, though they appeared potentially quite complicated. In an experiment at an intermediate velocity (523 m/s [figure 19]), the extruded ligament was tearing while extending, and ultimately the fracture was in a helical or corkscrew geometry. Much of the behavior during extrusion and exit appeared fluid-like. However, recovered failed specimens (figure 20) showed that the torn ligament recovered approximately to its original configuration. This indicated that the behavior was in fact solid-like. At high rates it appeared fluid-like due to very low stiffness. The final deformed PC shapes for the experiments performed at different velocities are shown in figure 20. Below impact velocities of 500 m/s, PC exhibited no fracture, little plastic deformation, and did not completely pass through the die exit. The simultaneous activity of void nucleation and coalescence combined with circumferential fracture was an intriguing result that deserves further study. Indeed, for ballistic applications, if two such mechanisms interact during penetration, then the mechanics need to be systematically investigated in a controlled manner like that provided by Dyn-Ten-Ex.

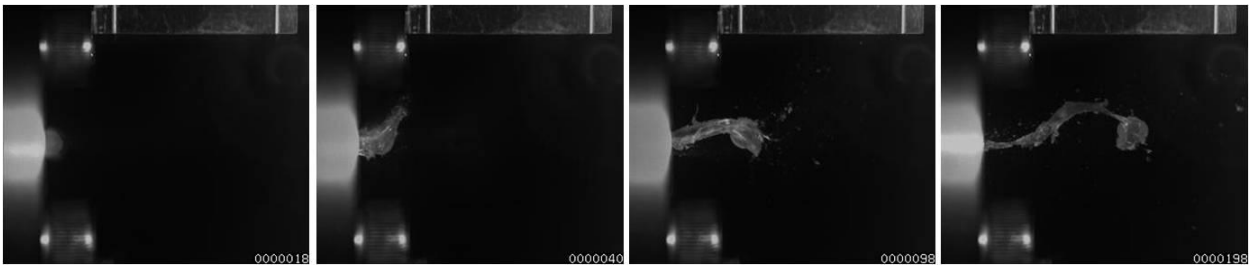

Figure 19. Dyn-Ten-Ext experiment for PC as captured at the die exit by a Shimadzu high-speed framing camera. The time in microseconds from camera trigger is noted in the lower-right corner of the images (18, 40, 98, and 198 μs, respectively). The test conditions were striking velocity of 523 m/s with a die exit of 0.36 cm. PC failure is in the corkscrew fracture/tearing mode. While it appears to behave in a molten fashion, the recovered pieces were found to have retracted almost to their original shape, indicating solid behavior.

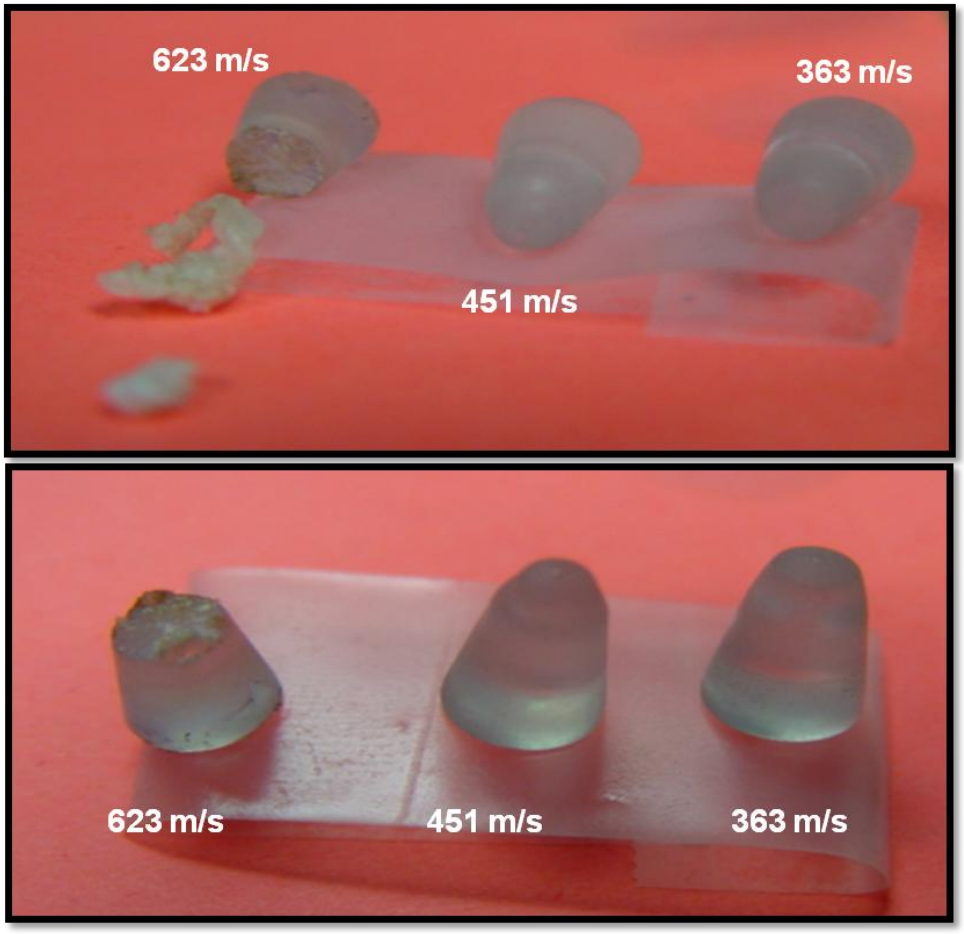

Figure 20. Recovered .30-caliber specimens from Dyn-Ten-Ext experiments for PC showing nearly complete elastic recovery (rebound) at 363 m/s; deformation near the exiting tip at 451 m/s; and failure with fracture above 600 m/s.

The experiment for the specimen striking at 363 m/s was chosen as the baseline case because it exhibited no failure and fracture. The complete VBB parameter set was used to activate all the competing mechanisms in the M-B model (called ‘VBB parameters’ in figures 21–23). As shown by the axial velocity plots in figure 21 for the VBB parameters column, the hemisphere ended PC cylinder made contact with the rigid die at approximately 5 μs and began to exit the die after 30 μs. At 40 μs the .30-caliber PC bullet stopped stretching and deforming in the axial direction and began to rebound back into the die (elastic recovery). Also, the highest axial velocity began to localize near the tip after 20 μs. A peak strain rate of approximately 3.5e+05/s was predicted near the contact region at early times (less than 20 μs) and then dropped to 10/s near the exit. For the ‘no pressure’ results shown in figure 21, similar trends were observed, but the bullet stretched further past the exit as compared with VBB. This is because the pressure dependent strength term for both viscoplastic dashpots was disabled which decreased strength or increased thermally activated deformation, thus predicting more deformation. When the alpha viscoplastic dashpot was disabled, as shown in figure 21 ‘no alpha,’ the flow strength dropped to values between 10 and 40 MPa and was dramatically under-predicted at low strain rates. For the ‘no beta’ case shown in figure 21, the beta dashpot was disabled and the flow strength at high strain rates reached values 20–25 MPa below the baseline value. In general, differences in deformation encountered for the Dyn-Ten-Ext predictions by disabling either viscoplastic dashpot follow the path for rate dependence of strength, as shown in figure 8 (b) for each viscoplastic component. Disabling the viscoplastic deformation mechanisms lowered the strength and resulted in higher deformation than the baseline case (VBB parameters) as well as for the no pressure case. The flow began to separate after exiting the die for the no alpha and no beta cases and resembled fracture even though no failure model was described in the input deck.

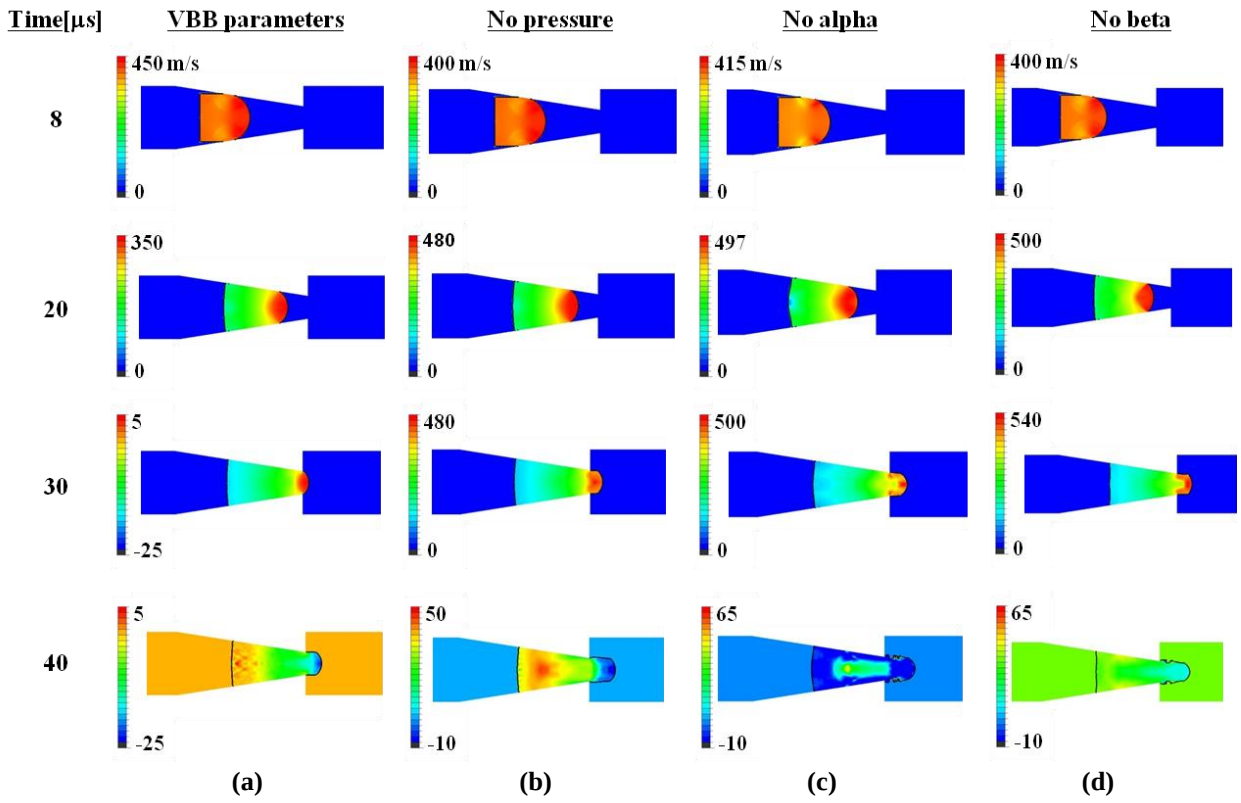

Figure 21. Parameter sensitivity showing numerical contours of velocity using the M-B model for a Dyn-Ten-Ext experiment at a striking velocity of 363 m/s at sequential times after die impact. (a) Full VBB parameters used in M-B, (b) VBB parameters used in M-B with pressure dependence of strength disabled, (c) VBB parameters used in M-B with the viscoplastic α phase disabled, and (d) VBB parameters used in M-B with the viscoplastic β phase disabled.

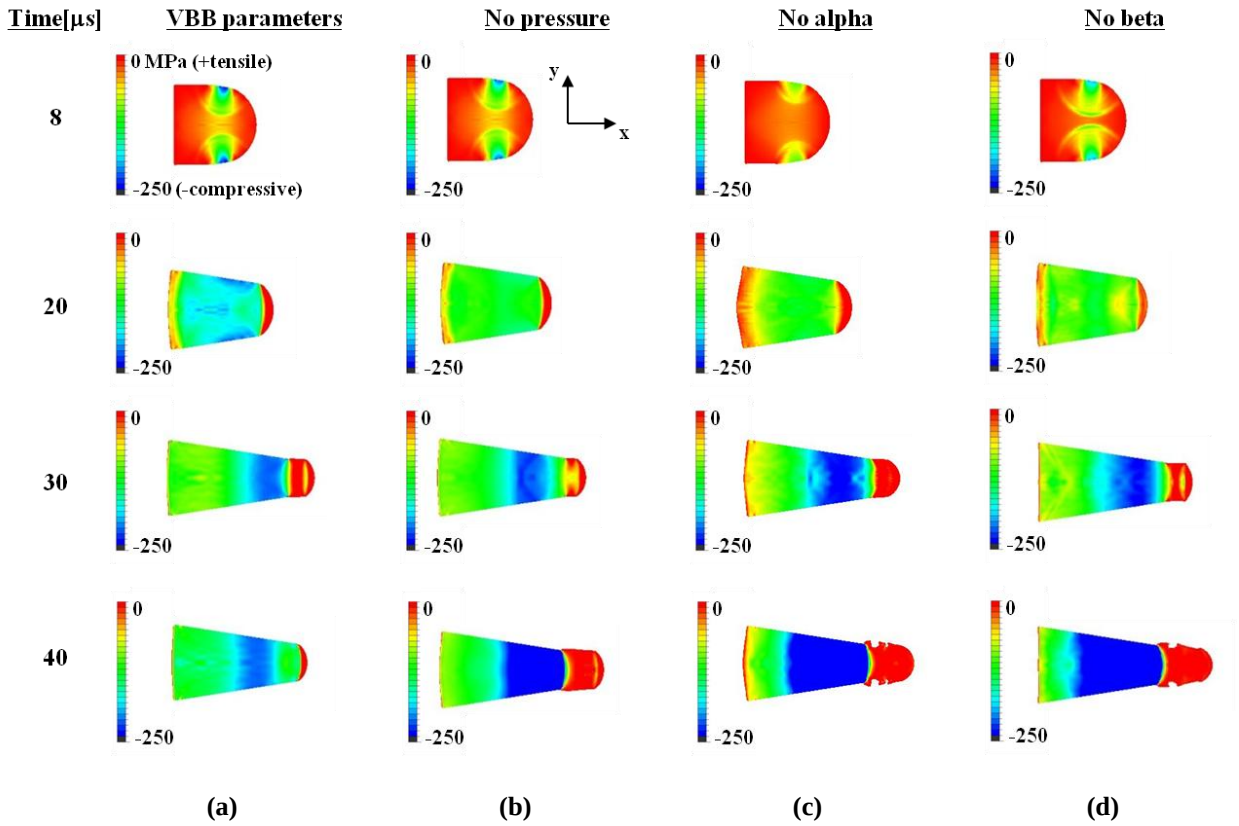

Figure 22. Parameter sensitivity showing numerical contours of radial stress using the M-B model for a Dyn-Ten-Ext experiment at a striking velocity of 363 m/s at sequential times after die impact. (a) Full VBB parameters used in M-B, (b) VBB parameters used in M-B with pressure dependence of strength disabled, (c) VBB parameters used in M-B with the viscoplastic α phase disabled, and (d) VBB parameters used in M-B with the viscoplastic β phase disabled. Note, positive stress is tensile and negative is compressive.

Figures 22 and 23 show the evolution of stress tensor components as a function of the parametric parameter sensitivity analysis. Radial stress for the PC bullet began to emanate at the region of contact with the angled die, as shown in figure 22 VBB parameters at 8 μs. By 20 μs the tip of the bullet exhibited negligible stress because it was a free end while the center region was being squeezed from the sides in a compressive state, as shown in figures 22 and 23. As it began to exit the die at 30 μs, the tip remained stress free but now a highly compressed region formed immediately behind it, as shown in figure 22 VBB parameters at 30 μs. This compressive wave eventually moved down toward the back end and reflected in tension as the tip began to rebound (elastic recovery). It was during this stage that having the slide line for the rigid die tied to the bullet, caused the timestep to decrease.

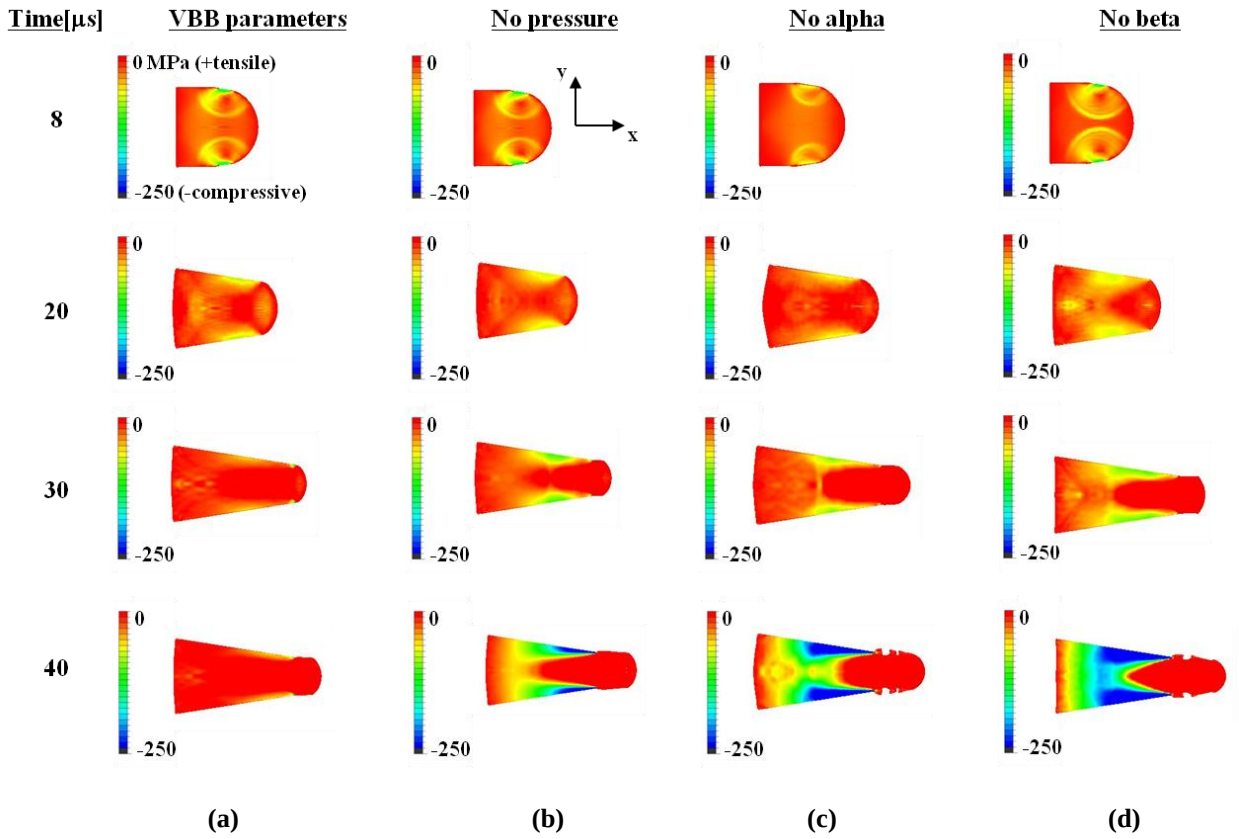

Figure 23. Parameter sensitivity showing numerical contours of axial stress using the M-B model for a Dyn-Ten-Ext experiment at a striking velocity of 363 m/s at sequential times after die impact. (a) Full VBB parameters used in M-B, (b) VBB parameters used in M-B with pressure dependence of strength disabled, (c) VBB parameters used in M-B with the viscoplastic α phase disabled, and (d) VBB parameters used in M-B with the viscoplastic β phase disabled. Note, positive stress is tensile and negative is compressive.

For the no alpha and no beta cases shown in the axial stress plots of figure 23 at 40 μs, an increase in radial compression as compared with the no pressure case evolved in the die contact region during rebound (elastic recovery) of the PC bullet. By disabling either viscoplastic term, the region of increased flow stress was due to high compressive strains from the chain stretching term in segment B. To verify this, numerical output was data reduced to calculate the stress due to chain stretching for three locations of the bullet at 40 μs. The highest stress due to chain stretch was located directly behind the tip at approximately 220 MPa, dropping to moderate values of approximately 130 MPa at the midsection and the smallest values of approximately 5 MPa at the rear of the hemisphere bullet.

Additionally, the modified M-B model accounted for plastic work-to-heat conversion resulted in a temperature increase of approximately 32 K for all cases examined. The increase in temperature due to plastic deformation was similar in dynamic tension and dynamic compression and is an important feature for simulations of any ballistic event.

6. Summary, Conclusions and Recommendations

The M-B constitutive model for amorphous glassy polymers includes three competing intermolecular deformation mechanisms that together describe material response from low to high strain rates. One mechanism describes chain alignment or stretching using an elastic only hardening condition that is not dependent on strain rate or temperature. The remaining two mechanisms are thermally activated energy equations for chain rotation at low and high strain rates, respectively. The chain rotation mechanisms describe thermal softening that is rate and temperature dependent including the temperature rise due to energy dissipation from the conversion of plastic work to heat.

A parameter sensitivity analysis was completed using a modified form of the M-B model to determine the influence of competing, multiple mechanisms of deformation for PC when subjected to extreme thermo-mechanical states. Isolated loading conditions for dynamic compression and dynamic tension traditionally applied for model validation, were used for numerical comparisons and analysis. A parametric study was completed by individually disabling three modes of deformation: pressure dependent flow strength, thermal softening at low strain rates (α-chain rotation viscoplastic term), and thermal softening at high strain rates (β-chain rotation viscoplastic term).

For dynamic compression, the complete VBB parameter set was compared with the original parameters used in the M-B model. Small differences in the final deformed shape between the two parameter sets as compared with the Taylor cylinder impact experiments were attributed to using modified viscoplastic VBB model parameters that accounted for the temperature rise from the conversion of plastic work to heat (deformation heating) and the shear modulus being split into two parts using an energy-based equation-of-state. The influence of pressure on flow strength was examined by disabling pressure dependence in M-B. PC exhibited no change in deformation with pressure dependence disabled when subjected to dynamic compression for strain rates at or below 10^5/s. For events occurring at higher strain rates, pressure dependence is expected to exhibit greater influence on deformation. When the α-chain rotation term was disabled the flow stress was nearly zero below the uniaxial stress data at 10^2/s and increased above the 10^2/s level due to the β-chain rotation term (but still below the observed rate sensitive yield stress). For this case, the Langevin spring had the greatest influence on deformation resulting with an increase in strain hardening along the axis of the cylinder (as evidenced by an equivalent increased zone of chain stretching along the axis). When the β-chain rotation term was disabled the flow stress was 10–20 MPa below the observed uniaxial results for strain rates above 10^2/s. For this case, thermal softening due to α-chain rotation had the greatest influence resulting with increased radial barreling.

For behavior in dynamic tension using the Dyn-Ten-Ext experiment, disabling pressure dependence or either viscoplastic dashpots numerically lowered the dynamic yield strength of PC, which resulted in larger displacement through the die exit. When the viscoplastic dashpots were disabled, it revealed the largest deformations and the formation of a large compressive zone with increasing flow stress due to chain stretching directly behind the tip of the bullet during elastic recovery (rebounding stage).

Recommendations for future work include parameter sensitivity analysis using dynamic shear and obtaining a new set of VBB parameters for M-B by considering a 50–60% conversion of plastic work to heat (*22, 23*). Model predictions were also examined when the initial temperature of PC was at or above the glass transition temperature, T_g. When the initial temperature was 20 K below T_g, the code had difficulties as specimen temperature increased due to energy dissipation from plastic work. Essentially, it could not decide if the amorphous polymer was in the soft or solid phase and localized high strain rates appeared temporally in random elements. An extension of the M-B model through the glass transition region is recommended for improved effectiveness toward predicting deformation states at extreme environments. Additionally, the Langevin spring describing molecular chain stretching assumed elastic hardening that is completely recovered. Experiments that closely monitor recovery may uncover a nonreversible portion for chain stretching that would promote modifications to segment A in M-B.

The most general product of this research effort was to offer an alternative purpose for experiments conventionally used to validate constitutive models. Although model validation is necessary, investing time "adjusting" model parameters to match observed results can always be accomplished, as long as the observed comes first (*24*). But the value of this investment will have small returns when applied at extreme ballistic environments. Instead, it is recommended to use model validation of an experiment as the baseline case for performing model parameter sensitivity, as illustrated in this report. Far more physical understanding of competing deformation mechanisms as described within physics-based constitutive models can be achieved that become relevant for uncovering protection defeat mechanisms at ballistic regimes. An additional relevant sensitivity analysis would involve altering the functional forms of terms described in a constitutive model for uncovering protection effectiveness as related to property performance. Together, this approach is an important ingredient toward achieving goals for protection-by-design involving material processing and fabrication to performance.

7. References

1. Reed, H. *Ballisticians in War and Peace: A History of the United States Army Ballistic Research Laboratory*; U.S. Army Research Laboratory: Aberdeen Proving Ground, MD, 1992; Vol. 3.

2. Burns, B. *Advanced Ballistics Science and Engineering*; ARL-SR-168; U.S. Army Research Laboratory: Aberdeen Proving Ground, MD, 2008.

3. Nichols, A. L. *Users Manual for ALE3D: An Arbitrary Lagrange/Eulerian 2-D and 3-D Code System*; Lawrence Livermore National Laboratory: Livermore, CA, 2009.

4. Walley, S. M.; Field, J. E.; Blair, P. W.; Milford, A. J. The Effect of Temperature on the Impact Behaviour of Glass/Polycarbonate Laminates. *Int. J. Imp. Eng*. **2004,** *30*, 31–53.

5. Funk, D. J.; Gray, R.; Germann, T.; Martineau, R. *A Summary Report on the 21st Century Needs of Compression Science Workshop*; Los Alamos National Laboratory Report LA-UR-09-07771: Santa Fe, NM, 2009.

6. Wilkins, M. L.; Cline, C. F.; Honodel, C. A. *Fourth Progress Report of Light Armor Program, UCRL-50694*; Lawrence Radiation Laboratory: Livermore, CA, 1969.

7. Hawkyard, J. B.; Eaton, D.; Johnson, W. The Mean Dynamic Yield Strength of Copper and Low Carbon Steel at Elevated Temperatures from Measurements of the ‘Mushrooming’ of Flat-Ended Projectiles. *Int. J. Mech. Sci*. **1968,** *10*, 929–948.

8. Cao, F.; Cerreta, E. K.; Trujillo, C. P.; Gray, G. T., III Dynamic Tensile Extrusion Response of Tantalum. *Acta Materialia* **2008,** *56*, 5804–5817.

9. Gray, G. T., III; Cerreta, E. K.; Yablinsky, C. A.; Addessio, L. B.; Henrie, B. L.; Sencer, B. H.; Buckett, M.; Maudlin, P. J.; Maloy, S. A.; Trujillo, C. P.; Lopez, M. F. Influence of Shock Prestraining and Grain Size on the Dynamic-Tensile-Extrusion Response of Copper: Experiments and Simulation. *Proc. of APS Shock Compression of Condensed Matter*, Baltimore, MD, 2005.

10. Mulliken, A. D. Mechanics of Amorphous Polymers and Polymer Nanocomposites During High-Rate Deformation. Doctoral Thesis, Massachusetts Institute of Technology, 2006.

11. Sarva, S.; Mulliken, A. D.; Boyce, M. C. Mechanics of Taylor Impact Testing of Polycarbonate. *Int. J. Sol. Struct.* **2007,** *44*, 2381–2400.

12. Maudlin, P. J.; Gray, G. T., III; Cady, C. M.; Kaschner, G. C. High-Rate Material Modeling and Validation Using the Taylor Cylinder Impact Test. *Phil. Trans. R. Soc. Lond. A.* **1999,** *357*, 1707–1729.

13. Eyring, H.; Viscosity, Plasticity, and Diffusion as Examples of Absolute Reaction Rates. *J. Chem. Phys*. **1936,** *4*, 283–291.

14. Ree, T.; Eyring, H. Theory for Non-Newtonian Flow I. Solid Plastic System. *J. Appl. Phys*. **1955,** *26*, 793.

15. Bauwens, J. Relation Between the Compression Yield Stress and the Mechanical Loss Peak of Bisphenol-A-Polycarbonate in the β Transition Range. *J. Matls. Sci*. **1972,** *7*, 577–584.

16. Mulliken, A. D.; Boyce, M. C. Mechanics of the Rate-Dependent Elastic-Plastic Deformation of Glassy Polymers from Low to High Strain-Rates. *Int. J. Sol. Struct*. **2006,** *43*, 1331–1356.

17. Arruda, E.; Boyce, M. C. Evolution of Plastic Anisotropy in Amorphous Glassy Polymers During Finite Straining. *Int. J. Plas*. **1993,** *9*, 697–720.

18. Varghese, A. G.; Batra, R. C. Constitutive Equations for Thermomechanical Deformations of Glassy Polymers. *Int. J. Sol. Struct*. **2009,** *46*, 4079–4094.

19. Nimmer, R. P.; Woods, J. T. An Investigation of Brittle Failure in Ductile Notch-Sensitive *Thermo-plastics. Pol. Eng. Sci*. **1992,** *32*, 1126–1137.

20. Johnson, M. D. Deformation and Fracture of Polycarbonate and Rubber-modified Polycarbonate Under Controlled Temperature, Deformation Rate, and Notch Stress Triaxiality. Doctoral Thesis, Massachusetts Institute of Technology, 2001.

21. Socrate, S.; Boyce, M. C. Micromechanics of Toughened Polycarbonate. *J. Mech. Phys. Solids* **2000,** *48*, 233–273.

22. Li, Z.; Lambros, J. Strain Rate Effects on the Thermomechanical Behavior of Polymers. *Int. J. Sol. Struct*. **2001,** *38*, 3549–3562.

23. Rittel, D. On the Conversion of Plastic Work to Heat During High Strain Rate Deformation of Glassy Polymers. *Mech. Matls*. **1999,** *31*, 131–139.

24. Zukas, J. U.S. Army Ballistic Research Laboratory, Aberdeen Proving Ground, MD. Private communication, 1998.

1 (PDF) DEFENSE TECHNICAL INFORMATION CTR DTIC OCA

2 (PDF) DIRECTOR US ARMY RESEARCH LAB RDRL CIO LL IMAL HRA MAIL & RECORDS MGMT

1 (PDF) GOVT PRINTG OFC A MALHOTRA

2 (PDF) LAWRENCE LIVERMORE NATL LAB A ANDERSON D FAUX

2 (PDF) PICATINNY ARSENAL ARDEC RDAR DIM E BAKER RDAR DSM D CARLUCCI

ABERDEEN PROVING GROUND

56 (10 HC) (46 PDF) DIR USARL
RDRL CIH C
J CAZAMIAS
D GROVE
RDRL DPW
R COATES
RDRL WM
P BAKER
B FORCH
S KARNA
RDRL WML
M ZOLTOSKI
RDRL WML H
J NEWILL
B SCHUSTER
RDRL WMM
J BEATTY
R DOWDING
J ZABINSKI
RDRL WMM B
R CARTER
B CHEESEMAN
B LOVE
C-F YEN
RDRL WMM D
S WALSH
RDRL WMM G
J ANDZELM
T CHANTAWANSRI
A HSIEH
RDRL WMP
D LYON
S SCHOENFELD
RDRL WMP A
D POWELL
RDRL WMP B
C HOPPEL
M LYNCH
RDRL WMP C
T BJERKE
R BECKER
S BILYK (10 HC)
RDRL WMP D
A BARD
R DONEY
D KLEPONIS
J RUNYEON
S SCHRAML
B SCOTT
RDRL WMP E
M BURKINS
D HACKBARTH
E HORWATH
T JONES
M KORNECKI
C KRAUTHAUSER
P SWOBODA
RDRL WMP F
N GNIAZDOWSKI
R GUPTA
RDRL WMP G
T DIGLIANI
N ELDREDGE
S KUKUCK